T CELLS



# Resident $T_H2$ cells orchestrate adipose tissue remodeling at a site adjacent to infection

**Agnieszka M. Kabat[1,2], Alexandra Hackl[1]†, David E. Sanin[1,2]†, Patrice Zeis[1,3,4]†, Katarzyna M. Grzes[1,2], Francesc Baixauli[1], Ryan Kyle[1], George Caputa[1], Joy Edwards-Hicks[1], Matteo Villa[1], Nisha Rana[1], Jonathan D. Curtis[1,2], Angela Castoldi[1], Jovana Cupovic[1], Leentje Dreesen[5], Maria Sibilia[6], J. Andrew Pospisilik[7], Joseph F. Urban Jr.[8], Dominic Grün[1,9,10,11], Erika L. Pearce[1,2,12], Edward J. Pearce[1,2,4,13]***

**Type 2 immunity is associated with adipose tissue (AT) homeostasis and infection with parasitic helminths, but whether AT participates in immunity to these parasites is unknown. We found that the fat content of mesenteric AT (mAT) declined in mice during infection with a gut-restricted helminth. This was associated with the accumulation of metabolically activated, interleukin-33 (IL-33), thymic stromal lymphopoietin (TSLP), and extracellular matrix (ECM)–producing stromal cells. These cells shared transcriptional features, including the expression of *Dpp4* and *Pi16*, with multipotent progenitor cells (MPC) that have been identified in numerous tissues and are reported to be capable of differentiating into fibroblasts and adipocytes. Concomitantly, mAT became infiltrated with resident T helper 2 ($T_H2$) cells that responded to TSLP and IL-33 by producing stromal cell–stimulating cytokines, including transforming growth factor β1 ($TGFβ_1$) and amphiregulin. These $T_H2$ cells expressed genes previously associated with type 2 innate lymphoid cells (ILC2), including *Nmur1*, *Calca*, *Klrg1*, and *Arg1*, and persisted in mAT for at least 11 months after anthelmintic drug–mediated clearance of infection. We found that MPC and $T_H2$ cells localized to ECM-rich interstitial spaces that appeared shared between mesenteric lymph node, mAT, and intestine. Stromal cell expression of epidermal growth factor receptor (EGFR), the receptor for amphiregulin, was required for immunity to infection. Our findings point to the importance of MPC and $T_H2$ cell interactions within the interstitium in orchestrating AT remodeling and immunity to an intestinal infection.**

## INTRODUCTION

There is a growing appreciation that lasting inflammation-induced changes in tissue homeostasis are mediated by nonhematopoietic cells in addition to resident immune cells. Communication between these two compartments is essential for host protection and subsequent reinforcement of tissues against secondary infections (*1*). In type 2 immune responses, cooperation between tissue-resident immune cells and nonhematopoietic cells ensures successful defense against pathogens (*2*, *3*) but when dysregulated can drive allergic and asthmatic inflammation, resulting in permanent fibrotic remodeling of the tissue (*4*). Nonimmune cells, such as epithelial and stromal cells, release signals including interleukin-25 (IL-25), IL-33, and thymic stromal lymphopoietin (TSLP), which are critical for the activation and maintenance of type 2 immune cells (*3*, *5*).

Type 2 immune processes underlie aspects of tissue homeostasis. This is particularly well recognized in adipose tissue (AT), where eosinophils and type 2 innate lymphoid cells (ILC2) contribute to the maintenance of alternative macrophage activation and are implicated in AT beiging and the prevention of metabolic disease (*6*–*9*). Regulatory T ($T_{reg}$) cells are also important for AT homeostasis (*10*, *11*). Stromal cells within visceral white AT produce IL-33, which activates and sustains ILC2 and $T_{reg}$ populations during homeostatic conditions (*12*–*15*). The stromal cell population in AT is heterogeneous, containing precursor cells in various stages of commitment to the adipocyte lineage (*16*). Recent work has identified multipotent progenitor cells (MPC), present in numerous tissues, that are capable of giving rise to multiple fibroblast subsets (*17*). MPC share a transcriptional signature, marked by *Dpp4*, *Pi16*, and *CD55* expression, with the cell type that gives rise to committed preadipocytes (*16*). Consistent with this, lineage tracing studies confirmed fibroblasts as the cell type that differentiates to adipocytes in vivo (*18*). However, it remains unclear how perturbations such as type 2 inflammation affect the structure and function of stromal cell populations within AT. It is of interest that AT MPC have been localized to interstitial tissue at the edge of AT and around the blood vessels (*16*, *18*), because IL-33–producing stromal cells

[1]Max Planck Institute for Immunobiology and Epigenetics, Freiburg 79108, Germany. [2]Bloomberg Kimmel Institute and Department of Oncology, Johns Hopkins University School of Medicine, Baltimore, MD 21287, USA. [3]International Max Planck Research School for Molecular and Cellular Biology (IMPRS-MCB), Freiburg, Germany. [4]Faculty of Biology, University of Freiburg, Freiburg 79104, Germany. [5]Department of Pathology and Immunology, Washington University School of Medicine, St. Louis, MO 63110, USA. [6]Institute of Cancer Research, Medical University of Vienna, Comprehensive Cancer Center, Borschkegasse 8a, Vienna A-1090, Austria. [7]Center for Epigenetics, Van Andel Research Institute, Grand Rapids, MI 49503, USA. [8]USDA, Agricultural Research Service, Beltsville Human Nutrition Research Center, Diet, Genomics, and Immunology Laboratory, and Belstville Agricultural Research Service, Animal Parasitic Disease Laboratory, Beltsville, MD 20705, USA. [9]Centre for Integrative Biological Signaling Studies (CIBSS), University of Freiburg, Freiburg 79104, Germany. [10]Würzburg Institute of Systems Immunology, Max Planck Research Group at the Julius-Maximilians-Universität, Würzburg 97078, Germany. [11]Helmholtz Institute for RNA-based Infection Research (HIRI), Helmholtz-Center for Infection Research (HZI), Würzburg 97080, Germany. [12]Department of Biochemistry and Molecular Biology, Johns Hopkins University Bloomberg School of Public Health, Baltimore, MD 21287, USA. [13]Department of Molecular Microbiology and Immunology, Johns Hopkins University Bloomberg School of Public Health, Baltimore, MD 21287, USA.
*Corresponding author. Email: epearce7@jhmi.edu
†These authors contributed equally to this work.

have also been identified to occupy interstitial niches in adventitia around blood vessels (*19*) and in the fascia of the skin (*20*).

Parasitic helminths, including the intestinal nematode *Heligmosomoides polygyrus bakeri* (*H. polygyrus*), induce strong type 2 immune responses, and resistance to reinfection with this parasite is dependent on adaptive type 2 immunity (*21*). Infection with *H. polygyrus* and other helminths prevents the development of obesity in mice fed a high-fat diet through an IL-33–dependent pathway linked to AT beiging (*6*, *9*, *22*–*24*). However, little is known about the development of adaptive type 2 immunity and T helper 2 ($T_H2$) cells in AT or the potential for AT to contribute to protective responses against helminth infection. This is of interest because there is a growing understanding that AT can be repurposed to participate in host defense against infection (*25*, *26*).

Mesenteric AT (mAT) is a white adipose depot that is closely associated with the intestinal tract and surrounds the vasculature, lymphatics, and mesenteric lymph nodes (mLNs) that drain the gut (*27*). When examining mice infected with *H. polygyrus*, we noted gross changes in the size and stiffness of mAT that suggested effects distal to the enteric site of infection. This prompted us to explore the biology of mAT over the course of *H. polygyrus* infection, recovery after treatment, and secondary *H. polygyrus* infection. Our data revealed dynamic changes in type 2 immunity, characterized by the development of a mAT-resident population of amphiregulin (Areg) and transforming growth factor β1 ($TGF\beta_1$)–producing $T_H2$ cells. This was paralleled by activation of the MPC compartment, underscored by increased production of the $T_H2$ cell–activating cytokines TSLP and IL-33 as well as increased extracellular matrix (ECM) secretion. We found that interstitial, ECM-rich niches, which are contiguous with the small intestine, became a site of $T_H2$ cell and MPC interactions. Our findings implicate stromal cell responses to Areg in resistance to *H. polygyrus* infection.

## RESULTS

### Dynamic changes occur in AT adjacent to the site of infection

We examined the effects of primary and secondary infection with *H. polygyrus* on mAT biology (fig. S1A). This infection is chronic but can be cleared by treatment with anthelmintic drugs such as pyrantel pamoate, after which mice show increased resistance to secondary challenge. We found that infection-induced mLN enlargement was accompanied by a reduction in surrounding mAT (Fig. 1A), characterized by a decrease in mAT weight and fat content, whereas food intake and total body weights between infected and control mice remained comparable (Fig. 1, B and C, and fig. S1, B and C). Although serum leptin levels were unaffected by infection, adiponectin levels declined, which was in line with the decrease in adiposity (fig. S1, D and E). We found that cellularity of the mAT stromal vascular fraction, particularly after secondary infection, was increased (Fig. 1D). These changes in stromal vascular fraction cellularity reflected increases in both immune and stromal cell numbers (Fig. 1, E and F, and fig. S1F).

We noted that infection caused an increase in stromal cell size and side scatter, indicating that these cells had become activated and potentially secretory (Fig. 1, G and H, and fig. S1G). To understand infection-associated changes in mAT stromal cells, we performed RNA sequencing (RNA-seq) on sorted $CD45^-$ $CD31^-$ $Sca1^+$ $PDGFR\alpha^+$ (platelet-derived growth factor receptor α–positive) stromal cells. Pathway enrichment analysis revealed an emphasis on ECM and inflammation, with expression of collagen, chemokine, and cytokine genes during infection (Fig. 1, I and J). Consistent with this, Masson's trichrome staining revealed the expansion of collagen-rich areas within the mAT of infected mice, often in proximity to tertiary lymphoid structures, also referred to as fat-associated lymphoid clusters (Fig. 1K). Moreover, procollagen 1 (pCol1) as well as TSLP and IL-33 were constitutively secreted by mAT stromal cells when cultured ex vivo (Fig. 1, L to N). Production of these proteins was greater after secondary infection than after primary infection. We did not observe a strong infection-linked increase in cytokine or collagen production by stromal cells isolated from the gonadal AT (gAT) of the same animals (fig. S1H).

The increased size, granularity, and secretory activity of stromal cells from infected mice suggested an increase in anabolic metabolism. In other stromal cells, activation to assume a secretory phenotype is supported by increased uptake of both glucose and glutamine and by increased glycolysis to facilitate anabolism (*28*–*30*). Our analysis revealed that mAT stromal cells, but not gAT stromal cells, from infected mice were broadly more metabolically active than those from control mice, with increased baseline oxygen consumption rates (OCR) and spare respiratory capacity (*31*), indicative of increased mitochondrial respiration (Fig. 1, O and P, and fig. S1I). Further, the extracellular acidification rate (ECAR), an indicator of lactate release as a result of glycolysis, was increased in mAT stromal cells from infected animals (Fig. 1Q). Metabolic activation was most pronounced in secondary infection (Fig. 1, O to Q). Moreover, metabolic activation was important for altered stromal cell function during infection because the selective glyceraldehyde phosphate dehydrogenase inhibitor heptelidic acid inhibited not only increased ECAR but also pCol1 and TSLP production by mAT stromal cells (Fig. 1, R to T). Together, these results indicate that *H. polygyrus* infection is associated with activation of the mAT stromal cell compartment.

### $T_H2$ cells with innate immune cell properties take up long-term residence in AT

We next explored infection-induced changes in the cellular composition of the mAT stromal vascular fraction in greater detail using single-cell RNA-seq (scRNA-seq). Unsupervised clustering of stromal vascular fraction cell transcriptomes revealed multiple cell clusters (C1 to C18; Fig. 2, A and B, and fig. S2, A and B). Infection-induced changes within the immune cell compartment were apparent, with a reduction in myeloid cells and an expansion of the $CD4^+$ T cell compartment (Fig. 2, B to D). These changes were confirmed by flow cytometry (Fig. 2, E and F, and fig. S2, C to G), which also revealed an increase, after secondary infection, of mAT eosinophils (Fig. 2G and fig. S2, D and H) that was not detected by scRNA-seq. To better resolve $CD4^+$ T cells and, in particular, *Gata3*-expressing cells, which would be expected to be involved in the recruitment of eosinophils, we performed an unsupervised reclustering of C4 and C9 and identified $T_H2$, $T_H1$, $T_{reg}$, ILC2, and natural killer T cells on the basis of canonical marker expression (fig. S3, A and B). The relative proportions of each cell type showed that numbers of $Gata3^+$ $T_H2$ cells increased during infection (fig. S3B).

Fluorescence-activated cell sorting (FACS) analysis confirmed that most mAT $CD4^+$ T cells in infected mice were $GATA3^+$ $FOXP3^-$ and therefore $T_H2$ cells (Fig. 2H and fig. S4A). mAT

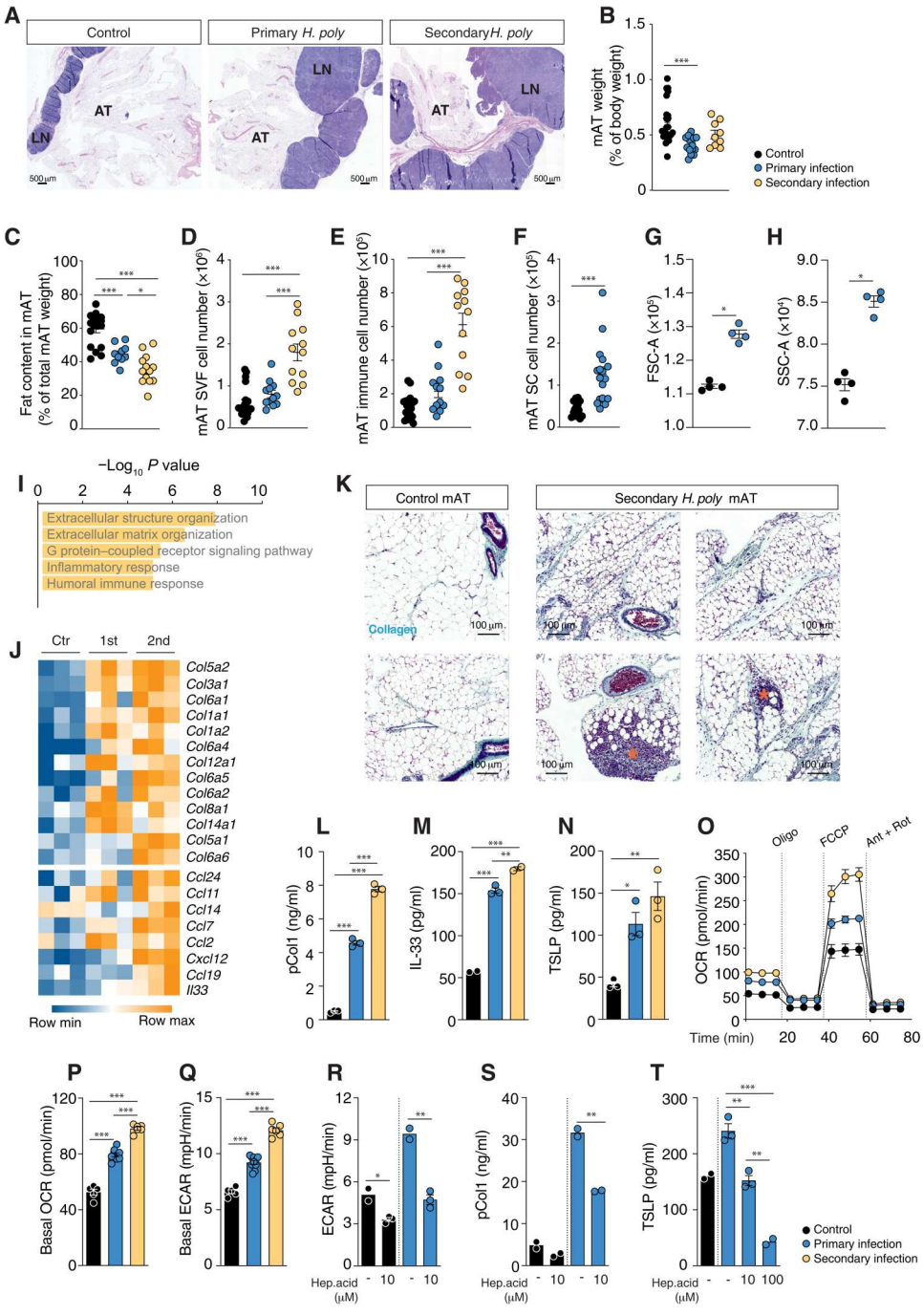


**Fig. 1. Extensive remodeling of mAT during *H. polygyrus* infection is associated with activation of the stromal cell compartment.** (**A**) H&E-stained sections of mAT and mLN in indicated experimental conditions. (**B**) mAT weights ($n$ = 9 to 23). (**C**) mAT fat content measured by MRI ($n$ = 10 to 18). (**D** to **F**) Counts of total stromal vascular fraction (SVF) cells (D, $n$ = 12 to 20), CD45$^+$ immune cells (E, $n$ = 12 to 20), and PDGFRα$^+$ Sca1$^+$ stromal cells (SC) (F, $n$ = 15 to 17). (**G**) mAT stromal cell size measured by flow cytometry. (**H**) mAT stromal cell granularity measured by flow cytometry. (**I** and **J**) RNA-seq of mAT stromal cells from control mice or mice with primary or secondary infection. Stromal cells were sorted from individual mice. (I) Gene Ontology enrichment analysis of significantly up-regulated genes (adjusted $P < 0.01$ and average $\log_{10}$ fold change > 0.25) in mice with primary *H. polygyrus* infection compared with control mice. (J) Heatmap indicating expression of selected genes of interest (collagens, cytokines, and chemokines) in control or infected mice. (**K**) Masson's trichrome staining of mAT sections from control or infected mice; collagen-enriched areas stain blue. Asterisks: fat-associated lymphoid clusters. (**L** to **N**) pCol1 (L), IL-33 (M), and TSLP (N) production by mAT stromal cells isolated from control or infected mice, measured in cell supernatants after overnight culture. (**O**) OCR of mAT stromal cells from indicated conditions at baseline and after sequential oligomycin (Oligo), FCCP, and rotenone/antimycin (Rot/Ant) injections, measured using Seahorse ($n$ = 5 to 10). (**P**) Baseline OCR of mAT stromal cells ($n$ = 5 to 10). (**Q**) Baseline ECAR of mAT stromal cells ($n$ = 5 to 10). (**R** to **T**) Effects of heptelidic acid on baseline ECAR (R), pCol1 (S), and TSLP production (T) of mAT stromal cells of control or infected mice. Data combined from two (A and F), three (C), or four (D and E) experiments, representative of two (A and O to S), three (G, H, K, N, and T), or four (L and M) experiments or from one experiment (I and J). Symbols represent biological (B to H) or technical (L to T) replicates. Mean ± SEM. *$P \leq 0.05$, **$P \leq 0.01$, ***$P \leq 0.001$. Data were analyzed by one-way unpaired ANOVA with Bonferroni's multiple comparison posttest (B to E, L to N, P, Q, and T), two-tailed unpaired $t$ test (R and S), or Mann-Whitney test (F to H).

$T_H2$ cells were characterized by high expression of receptors for the stroma-derived cytokines IL-33 and TSLP, whereas cells with these characteristics constituted only a small percentage of mLN cells (Fig. 2, H to K, and fig. S4, B to E). In secondary infection, up to 80% of all mAT CD4$^+$ T cells were FOXP3$^-$ GATA3$^+$ IL-33R$^+$ $T_H2$ cells (Fig. 2I and fig. S4A). We found that mAT $T_H2$ cells were CD69$^+$ CD44$^+$ and CD62L$^-$, suggesting that they were resident memory T cells ($T_{RM}$) (fig. S4F). *H. polygyrus* infection also increased the frequency of IL-33R$^+$ $T_H2$ cells within the CD4$^+$ T cell compartment of gAT, although the overall frequency of CD4$^+$ T cells did not change (fig. S4, G to J). Expansion of mAT deposits by high-fat diet feeding before infection did not affect the establishment of resident mAT $T_H2$ populations during infection (fig. S4K).

Previous studies located AT-resident T cells in fat-associated lymphoid clusters (*26*, *32*, *33*). In line with this, whole-mount mAT confocal microscopy revealed that numerous fat-associated lymphoid clusters, evident as dense clusters of nonadipocyte cells, were enriched in CD3$^+$ GATA3$^+$ ($T_H2$) cells in the infected mice (fig. S5, A and B). These structures were rare and smaller in mAT from uninfected mice. Moreover, in infected mice, $T_H2$ cells were also present not only in areas outside of the fat-associated lymphoid clusters, scattered among adipocytes and PDGFRα$^+$ stromal cells

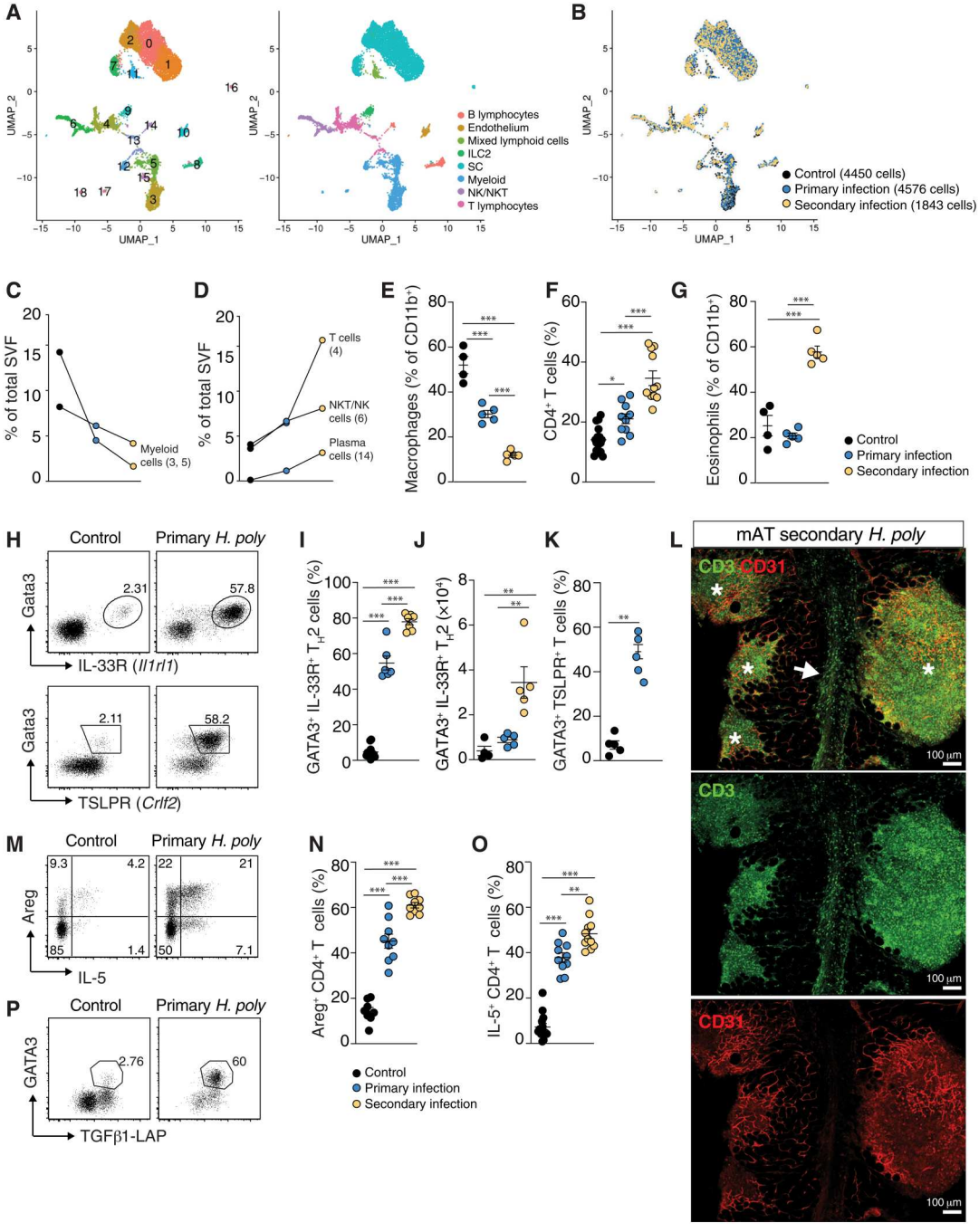


**Fig. 2. The mAT $T_H2_{RM}$ compartment expands during infection.** (**A** and **B**) Uniform manifold approximation and projection (UMAP) plots of 10,869 mAT stromal vascular fraction cells from a control mouse or mice with primary or secondary *H. polygyrus* infection (one mouse per condition). Unsupervised clustering identified 18 cell groups; plots are color-coded according to (A) cell cluster (left) and broad identification of cell types (right) or according to experimental condition (B). NK, natural killer cells; NKT, natural killer T cells. (**C** and **D**) Changes in immune cell populations after infection (normalized to total cell number in experimental condition). Numbers in brackets indicate cluster ID from (A). (**E** to **G**) Frequencies of mAT macrophages (F4/80$^{hi}$ SiglecF$^{low}$ of CD45$^+$ CD11b$^+$ cells) (E), CD4$^+$ T cells (CD4$^+$ TCRβ$^+$ of CD45$^+$ cells in lymphocyte gate, $n$ = 10 to 16) (F), and eosinophils (F4/80$^{low}$ SiglecF$^{hi}$ of CD45$^+$ CD11b$^+$ cells) (G) in control or infected mice, measured by flow cytometry. (**H** to **K**) Flow cytometry plots (H), frequencies (I and K), and numbers (J) of GATA3$^+$ IL-33R$^+$ and GATA3$^+$ TSLPR$^+$ $T_H2$ cells (gated on FOXP3$^-$ CD4$^+$ TCRβ$^+$ CD45$^+$ cells) in mAT from control or infected mice. (**L**) Whole-mount immunofluorescent images of mAT of infected mice stained for CD3 and CD31. Arrow: Interstitial space. Asterisks: fat-associated lymphoid clusters. (**M** to **O**) Flow cytometry plots (M) and frequencies of Areg (N, $n$ = 8 to 9) and IL-5 (O, $n$ = 10 to 14) expression by mAT CD4$^+$ T cells (gated on FOXP3$^-$ CD4$^+$ TCRβ$^+$ CD45$^+$ cells). (**P**) TGFβ1-latency associated peptide (LAP) expression by mAT $T_H2$ cells (gated on FOXP3$^-$ CD4$^+$ TCRβ$^+$ CD45$^+$ cells in lymphocyte gate). Data combined from two (I and N) or three (F and O) experiments, representative of two (E, G, and J to L) experiments, or from one experiment (A to D and P). Symbols represent biological replicates (E to G, I to K, N, and O). Mean ± SEM. $^{**}P \leq 0.01$ and $^{***}P \leq 0.001$. Data were analyzed by one-way unpaired ANOVA with Bonferroni's multiple comparison posttest (E to G, I, J, N, and O) or Mann-Whitney test (K).

(fig. S5, B and C), but also along the interstitial spaces (the adventitia and reticular interstitium), which appeared to connect with these lymphoid structures (Fig. 2L and fig. S6).

Functionally, most mAT GATA3$^+$ $T_H2$ cells from infected mice were capable of making not only the eosinophil survival factor IL-5 but also the tissue modulatory cytokines Areg and TGF$\beta_1$ (Fig. 2, M to P, and fig. S7, A and B); cells with these attributes were less frequent in the mLN from the same animals (fig. S7, C to E), consistent with the view that terminal $T_H2$ cell differentiation occurs within peripheral tissues (*34*). Our data also indicated that as a result of infection, Areg production in mAT shifted from the innate compartment, where it occurred mostly in ILC, to the T cell compartment, where it was primarily a function of $T_H2$ cells, although ILC2 still remained a source of Areg (fig. S7, F to I). scRNA-seq data additionally suggested that $T_H2$ cells also became a major source of TGF$\beta_1$ in mAT during secondary infection (fig. S7, J to L). We did not detect strong expression of *Areg*, the gene encoding Areg, in myeloid cells (fig. S7, J to L). Last, we found that the increase in the $T_H2_{RM}$ population was also paralleled by the progressive infection-associated decline in the frequencies of mAT $T_{reg}$ cells and interferon-γ (IFN-γ)–producing CD4$^+$ T cells (fig. S8, A to E), suggesting that $T_H2$ cells may compete with $T_{reg}$ and $T_H1$ cells for available space in the mAT lymphoid niche. In this context, we noted that IL-33R was more strongly expressed by mAT $T_H2$ cells than mAT $T_{reg}$ cells in infected mice and that IL-33 intraperitoneal injection into naïve wild-type mice resulted in greater expansion of the $T_H2$ compared with $T_{reg}$ population in mAT (fig. S8, F to I), suggesting that $T_H2$ cells are more responsive to IL-33 than $T_{reg}$ cells.

To ask whether mAT $T_H2$ cells have tissue-specific attributes, we used scRNA-seq to compare them with $T_H2$ cells sorted from anatomically related sites affected by infection, namely, the small intestine and mLN. Clustering and similarity analysis with VarID (*35*) revealed distinct groupings of T cell populations by tissue of residence (Fig. 3, A and B). *Cd44*$^+$, *Cd69*$^+$, *Cd62l*$^-$ (*Sell*), and *Klf2*$^-$ $T_H2_{RM}$ cells were present in mAT and small intestine but nevertheless clustered separately from each other (C7 versus C11) (Fig. 3, A and C), indicating location-dependent functional distinctions. Previous work has described $T_H2_{RM}$ cells in small intestines and peritoneal cavities of *H. polygyrus*–infected mice but not in mAT (*36*). We observed that mAT, but not small intestine $T_H2_{RM}$ cells, up-regulated CD25 (*Il2ra*) and expressed high levels of *Il1rl1* (IL-33R, ST2), whereas small intestine $T_H2_{RM}$ cells displayed higher expression of *Il17rb* (IL-25R), reminiscent of tissue-specific alarmin receptor expression reported for ILC2 (Fig. 3D) (*37*). However, $T_H2_{RM}$ cells from mAT, to an equal or greater extent than small intestine $T_H2_{RM}$ cells, expressed several genes previously associated with ILC2: *Nmur1*, *Calca* (or *Cgrp*), *Klrg1*, and *Arg1*, indicating that $T_H2_{RM}$ cells acquire an innate-like phenotype when residing in mAT (Fig. 3D).

In contrast to small intestine $T_H2_{RM}$ cells, mAT $T_H2_{RM}$ cells expressed *Ccr2* (Fig. 3E), pointing toward a selective role for CCR2 ligands in $T_H2_{RM}$ cell localization in mAT. Moreover, analysis of integrin expression by both scRNA-seq and flow cytometry revealed that mAT $T_H2_{RM}$ cells did not express *Itgae* (CD103), a marker for many mucosal resident T cell populations (*38*), but did express *Itga4* (CD49d), unlike small intestine $T_H2$ cells (Fig. 3E and fig. S9A). Both $T_H2$ populations expressed *Itgb1* (CD29), *Itgb3* (CD61), and *Itgb7* (Fig. 3E and fig. S9A). This integrin expression pattern indicates that mAT $T_H2_{RM}$ cells can form functional heterodimeric integrin receptors that enable interactions with the stromal cells and ECM components. These findings, along with the fact that $T_H2_{RM}$ cells are found within the mAT stroma, suggest that they are motile within the tissue. Both mAT and small intestine $T_H2$ cells expressed *Il5*, *Il6*, *Areg*, and *Tgfb1*, but small intestine $T_H2$ cells expressed these genes, as well as *Il4* and *Il13*, more strongly than their mAT equivalents (Fig. 3F). This distinct cytokine expression pattern is again reminiscent of reported differences in ILC2, where intestinal ILC2 preferentially express IL-13 (*37*).

Consistent with mAT $T_H2$ cells being $T_{RM}$, $T_H2$ cell accumulation during secondary infection was unaffected by treatment with the sphingosine-1-phosphate receptor 1 (S1PR1) agonist FTY720 (Fig. 3, G to I), indicating that after primary infection the mAT $T_H2_{RM}$ population persisted independently from the recruitment of cells from secondary lymphoid organs through the S1PR1-dependent pathway. FTY720 treatment also had no effect on resistance to reinfection (Fig. 3J). Furthermore, mAT remained enriched in IL-33R$^+$ $T_H2_{RM}$ cells capable of making both IL-5 and Areg for up to 11 months after treatment (Fig. 3, K to M, and fig. S9, B and C), whereas $T_{reg}$ and ILC2 populations within this tissue were less frequent than those in naïve control mice throughout this time (Fig. 3, N and O, and fig. S9, D to H). The mAT $T_H2_{RM}$ population not only persisted but also continued to expand over time in the absence of infection (Fig. 3P). In summary, infection with *H. polygyrus*, an intestinal helminth parasite, led to the accumulation of $T_H2$ cells in mAT. These cells were phenotypically $T_H2_{RM}$-like, expressed receptors for the tissue alarmins IL-33 and TSLP, and made a range of tissue modulatory mediators, including Areg and TGF$\beta_1$.

## Resident $T_H2$ cells and stromal cells activate each other during infection

We asked how mAT $T_H2_{RM}$ cells influenced mAT remodeling during infection. Prevention of $T_H2$ cell development through the deletion of IL-4Rα on T cells in *Il4ra*$^{fl/fl}$ *Cd4*-Cre mice resulted in a reduction in resistance to secondary infection and the loss of associated components of the response such as tissue eosinophilia (Fig. 4, A to C, and fig. S10, A to C), confirming the importance of $T_H2$ cells for orchestrating type 2 immunity and host defense during secondary infection. When we examined mAT stromal cell activation in infected *Il4ra*$^{fl/fl}$ *Cd4*-Cre mice, we found that cytokine and pCol1 production was diminished compared with infected controls (Fig. 4, D and E), despite ILC2 and $T_{reg}$ cells still being present in mAT (fig. S10, A and D to G). Furthermore, stromal cell activation was also diminished when CD4$^+$ T cells were depleted, an intervention that also resulted in the loss of resistance to infection (Fig. 4, F to H, and fig. S10, H to K). $T_H2$ cells therefore played a critical role in mAT stromal cell activation during infection.

We next asked whether stromal cells reciprocally stimulated $T_H2_{RM}$ cells, by purifying and coculturing these populations and measuring $T_H2$ cell survival and cytokine production. We found that both were strongly enhanced in the presence of mAT stromal cells from infected or naïve mice (Fig. 4, I to K). These effects were seen when mAT $T_H2_{RM}$ cells and mAT stromal cells were cultured in a transwell system, indicating that soluble factor(s) from stromal cells could drive $T_H2_{RM}$ cell activation (fig. S10L). The expression of TSLPR and IL-33R on mAT $T_H2$ cells and the recognized relationship of TSLP and IL-33 with type 2 immunity suggested that it could be these cytokines that were responsible for the observed effects. To examine this possibility, we sorted both $T_H2$ cells (CD4$^+$Foxp3$^-$IL-

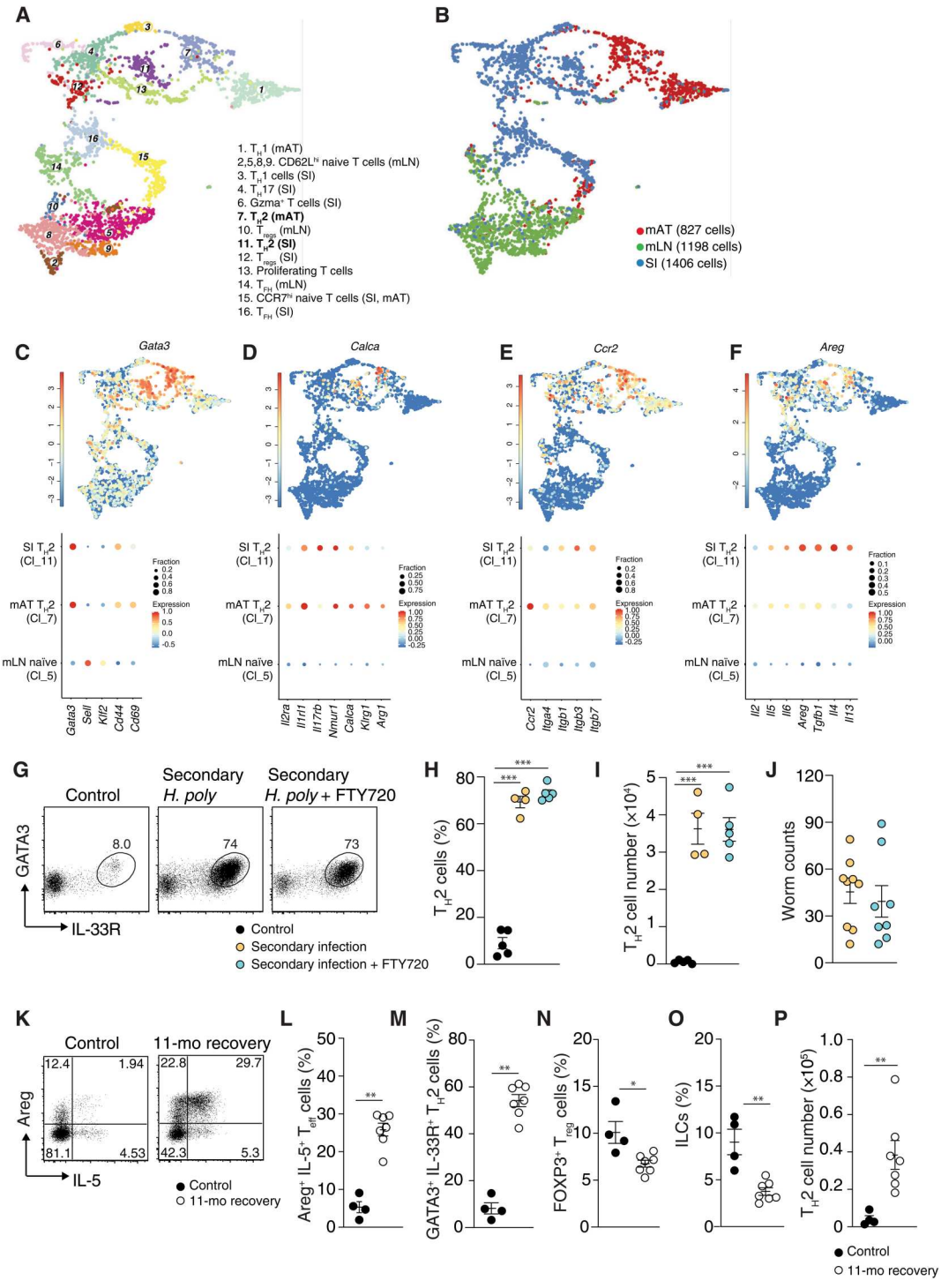


**Fig. 3. The mAT $T_H2$ cell population has innate cell properties, expands independently of T cell recruitment, and is long lived.** (**A** and **B**) UMAP plots of CD4$^+$ TCRβ$^+$ T cells from mLN and mAT of control ($n$ = 2 per condition), primary infected ($n$ = 1 per condition), and secondary infected ($n$ = 1 per condition) mice and from small intestine (SI) lamina propria of control and primary infected mice ($n$ = 2 per condition). Unsupervised clustering distinguished 16 cell groups; plots are color-coded according to cell identity (A) or tissue of origin (B). (**C** to **F**) UMAP plots indicating $\log_2$ normalized expression of selected genes of interest (top) and cluster-specific gene expression shown as dot plots (bottom), where color represents the $z$ score of the mean expression across clusters, and dot size represents the fraction of cells in the cluster expressing the selected gene. (**G** to **J**). Mice were given secondary infections and treated with FTY720 where indicated. Flow cytometry plots (G), frequencies (H), and numbers (I) of GATA3$^+$ IL-33R$^+$ $T_H2$ cells (gated on FOXP3$^-$ TCRβ$^+$ CD45$^+$ cells). Worm counts from small intestine (J). (**K** and **L**) Flow cytometry plots (K) and frequencies (L) of mAT IL-5$^+$ Areg$^+$ T cells (gated on FOXP3$^-$ CD4$^+$ TCRβ$^+$ CD45$^+$ cells). (**M** to **P**) Frequencies (M) and numbers (P) of mAT GATA3$^+$IL-33R$^+$ $T_H2$ cells and frequencies of $T_{reg}$ cells (FOXP3$^+$ CD4$^+$ TCRβ$^+$ CD45$^+$) (N) and ILCs (gated on Lin$^-$ CD45$^+$ Thy1$^+$ live cells in lymphocyte gate; see Materials and Methods) (O) after 11 months of recovery after treatment of primary infection. Data combined from two experiments (A to F and J) or representative of two experiments (G to P). Symbols represent biological replicates (H to J and L to P). Mean ± SEM. *$P \leq 0.05$, **$P \leq 0.01$, and ***$P \leq 0.001$. Data were analyzed by one-way unpaired ANOVA with Bonferroni's multiple comparison posttest (H and I) or Mann-Whitney test (J and L to P).

4$^+$) and non-$T_H2$/non-$T_{reg}$ cells (CD4$^+$Foxp3$^-$IL-4$^-$) from mAT and mLN of infected animals and cultured them in the presence or absence of IL-33 and TSLP. We found that mAT $T_H2_{RM}$ cells were more capable of surviving in vitro than non-$T_H2$/non-$T_{reg}$ cells or mLN $T_H2$ cells and that they proliferated extensively in the absence of added growth factors (Fig. 4L and fig. S10M). This distinction was further enhanced by the addition of IL-33 or TSLP (Fig. 4L and fig. S10M). We found that, without the ex vivo addition of a T cell receptor stimulus, TSLP and, in particular, IL-33 activated purified mAT $T_H2$ cells to produce Areg, IL-5, IL-6, IL-13, and TGFβ$_1$ (Fig. 4M and fig. S10N). We noted that whereas cytokine secretion by mAT $T_H2$ cells was driven more strongly by IL-33 (Fig. 4M), survival was enhanced more strongly by TSLP (Fig. 4L). These findings are consistent with the reported properties of these cytokines (*39*, *40*).

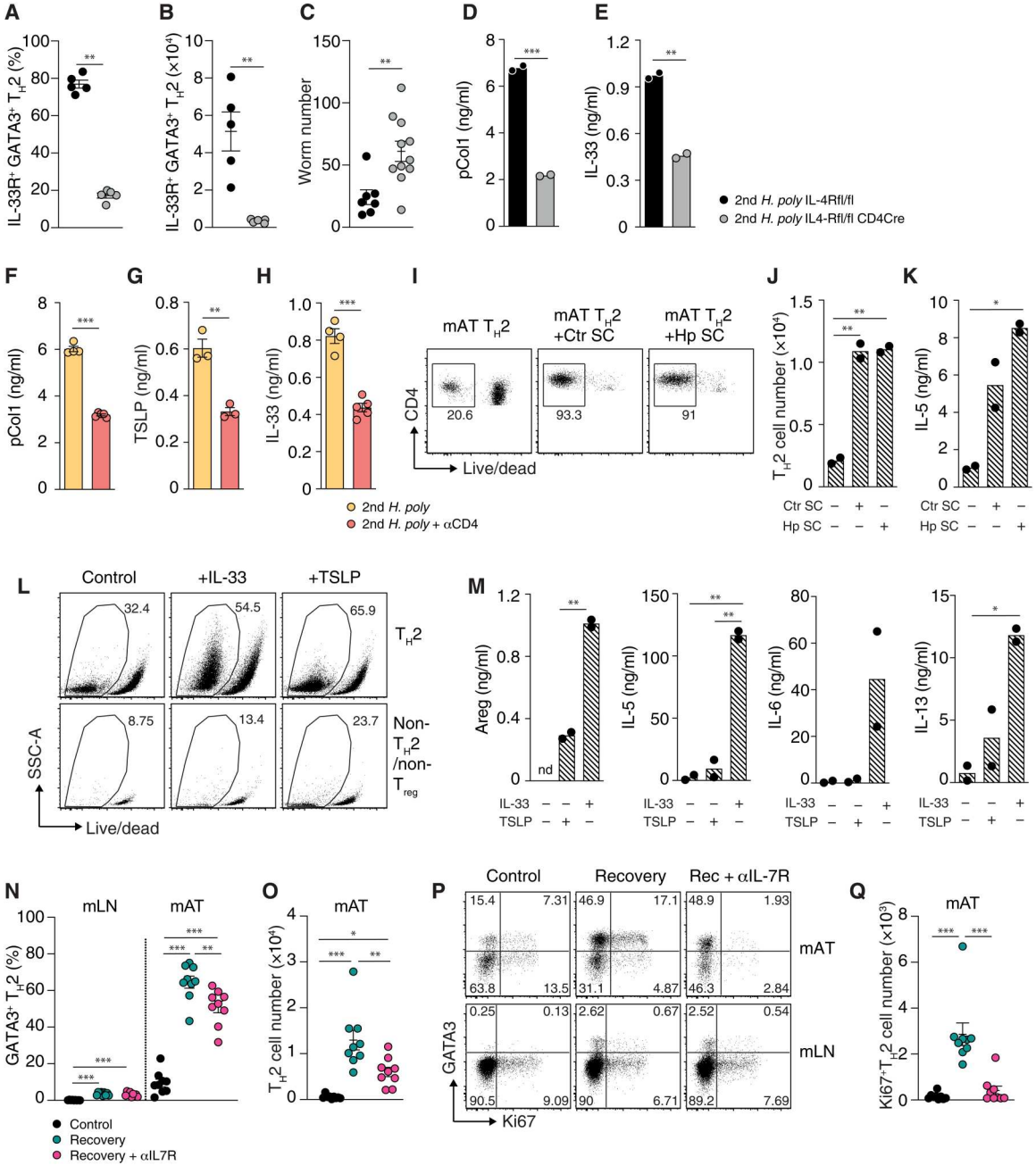


**Fig. 4. $T_H2_{RM}$ cells and stromal cells activate each other during *H. polygyrus* infection.** (**A** to **E**) *Il4ra*$^{fl/fl}$ *Cd4-Cre* and *Il4ra*$^{fl/fl}$ mice were subjected to secondary infection. Frequencies (A) and numbers (B) of mAT $T_H2$ cells (IL-33R$^+$ GATA3$^+$ FOXP3$^-$ CD4$^+$ TCRβ$^+$). (C) Worm numbers in small intestine. Production of pCol1 (D) and IL-33 (E) by mAT stromal cells isolated from *Il4ra*$^{fl/fl}$*Cd4-Cre* and *Il4ra*$^{fl/fl}$ mice. (**F** to **H**) pCol1 (F), TSLP (G), and IL-33 (H) production from isolated mAT stromal cells during secondary infection with anti-CD4 depletion where indicated. (**I** and **J**) Flow cytometry plot (I) and cell number (J) of sorted $T_H2$ cells after 4 days of coculture with mAT stromal cells isolated from uninfected or infected mice as indicated. (**K**) IL-5 production by $T_H2$ cells after 4 days of culture with mAT stromal cells as in (I). (**L** and **M**) $T_H2$ cells (CD4$^+$ TCRβ$^+$ IL4-eGFP$^+$ FOXP3RFP$^-$) and non-$T_H2$/non-$T_{reg}$ T cells (CD4$^+$ TCRβ$^+$ IL4-eGFP$^-$ FOXP3RFP$^-$) were sorted from mAT and mLN of infected mice and cultured for 3 to 6 days with addition of IL-33 (50 ng/ml) or TSLP (50 ng/ml). Flow cytometry plots of mAT $T_H2$ and non-$T_H2$/non-$T_{reg}$ cells with frequencies of live cells after 6 days of culture (L). Levels of indicated cytokines in the supernatants of mAT $T_H2$ cells after 3 days of culture (M). (**N** to **Q**) TSLP signaling was blocked with anti–IL-7Rα antibody treatment during recovery after primary infection. Frequencies (N, $n = 9$) and numbers (O, $n = 9$) of $T_H2$ cells (GATA3$^+$ FOXP3$^-$ CD4$^+$ TCRβ$^+$) in mAT or mLN as indicated. Flow cytometry plots (P) and numbers (Q, $n = 9$) of Ki67$^+$ $T_H2$ cells in mAT. Data combined from two experiments (C, N, O, and Q), representative of two (A, B, D, I, and K to M) or three (F and H) experiments or from one experiment (E, G, and J). Symbols represent biological (A to C and M to Q) or technical (D to K) replicates. Mean ± SEM. *$P \leq 0.05$, **$P \leq 0.01$, and ***$P \leq 0.001$. Data were analyzed by one-way unpaired ANOVA with Bonferroni's multiple comparison posttest (J, K, M to O, and Q), two-tailed unpaired *t* test (D to H), or Mann-Whitney test (A to C).

TSLP signals through a heterodimeric receptor consisting of CRLF2 and IL-7Rα, the latter of which, when paired with $\gamma_c$ (encode by *Il2rg*), is also a component of the bona fide IL-7R (*41*). $T_H2_{RM}$ cells expressed *Crlf2*, *Il7ra*, and *Il2rg*, suggesting that they could use TSLP or IL-7 for survival in the mAT niche (Fig. 2, H and K, and fig. S11, A to C). Consistent with this, antibody-mediated blockade of IL-7Rα for 1 week during post-infection recovery resulted in significant decreases in $T_H2$ cells and in $Ki67^+$ $T_H2$ cells in mAT, but not in mLN, confirming a requirement for TSLP/IL-7 signaling for mAT $T_H2_{RM}$ cell proliferation and persistence (Fig. 4, N to Q, and fig. S11D), although this treatment does not exclude indirect effects of IL-7Rα inhibition on other mAT-resident immune populations. Because we could not detect IL-7 in stromal cell culture supernatants and *Il7* was not strongly expressed by $Pdgfra^+$ stromal cells in the scRNA-seq data (fig. S11E), these results likely reflected the inhibition of TSLP-mediated effects. Together, our data point to the existence of a positive feedback loop in which $T_H2_{RM}$ cells in the mAT activate stromal cells to secrete IL-33 and TSLP, which in turn promote mAT $T_H2_{RM}$ cell expansion, survival, and cytokine production.

### Activated stromal MPC accumulate and secrete collagen and immunostimulatory cytokines

To more fully explore the mAT stromal response to infection, we reclustered the scRNA-seq stromal cell transcriptomes and identified six distinct cell groups (C0 to C5; Fig. 5A and fig. S12, A and B). Using published transcription profiles to delineate adipocyte differentiation stages, we identified $Dpp4^+$ $Pi16^+$ $CD55^+$ MPC (C2), intermediate uncommitted cells (C0), and $Fabp4^+$ $Pparg^+$ committed preadipocytes (C1) (*16*, *42*, *43*). Other clusters were enriched in $CD9^+$ matrix fibroblasts (C3) (*44*) and $Ccl19^+$ immunofibroblasts (C4) (Fig. 5A and fig. S12, A and B) (*45*). By pseudotemporal ordering using Monocle (*46*) with MPC (C2) set as the origin, our data conformed with the model proposed by others in which, within AT, committed preadipocytes capable of giving rise to mature adipocytes differentiate from $Dpp4^+$ uncommitted progenitor cells (Fig. 5B) (*16*). A quantitative assessment of cluster sizes revealed an ~25% increase in MPC (C2) and a decrease in intermediate uncommitted cells (C0) in infected versus control mice (Fig. 5C), suggesting a reduction in the differentiation of the MPC toward the adipocyte lineage.

We used flow cytometry to further investigate quantitative changes in mAT stromal cell populations. We gated on $CD45^-$ $CD31^-$ $Sca1^+$ $PDGFR\alpha^+$ stromal cells and used antibodies against surface molecules shown previously (*16*, *43*) to discriminate between MPC (Ly6c and Thy1), committed matrix fibroblasts (which more strongly express CD9 but not Ly6c), and committed preadipocytes (which are $CD9^{lo}Ly6c^{lo}$) (Fig. 5D). On the basis of these criteria, infection led to increased frequencies of MPC and reduced frequencies of committed subsets (Fig. 5, E to G). Furthermore, MPC numbers were increased significantly during infection (fig. S12C). This increase was dependent on $T_H2$ cells because it was diminished in infected $Il4ra^{fl/fl}$ *Cd4*-Cre mice (fig. S12D). Moreover, stromal cells from infected $Il4ra^{fl/fl}$ *Cd4*-Cre mice were less granular than those from infected controls, suggesting that stromal cell activation is generally $T_H2$ cell dependent (fig. S12, E and F). To verify functional differences between identified stromal subpopulations, we sorted them on the basis of Ly6c and CD9 expression (Fig. 5E) and asked which had the potential to become adipocytes under adipogenic culture conditions (*16*). We found that the committed preadipocytes had the highest adipogenic potential, evident by extensive lipid droplet development (evident as increased staining with Oil Red), whereas MPC showed intermediate adipogenic potential. The matrix fibroblast subpopulation contained few cells that were able to differentiate into mature adipocytes (Fig. 5H and fig. S12G). Infection did not affect the inherent ability of cells within the different stromal cell subpopulations to differentiate into mature adipocytes in culture (Fig. 5H and fig. S12G). These data confirmed the functional relatedness of the clusters identified in our study to previous descriptions of adipocyte differentiation (*16*, *43*, *44*).

We next asked whether infection-induced increases in collagen production could be attributed to a particular subpopulation of mAT stromal cells. We found that pCol1 was produced by sorted matrix fibroblasts and MPC and that both of these populations produced more pCol1 when sorted from infected mice (Fig. 5I). However, the MPC made more pCol1 than did the matrix fibroblasts, despite indications from the scRNA-seq data that the opposite would be the case. By comparison, committed preadipocytes from infected mice made little pCol1 (Fig. 5I). In addition, MPC were the major source of TSLP, production of which was greatly increased as a result of infection (Fig. 5J). We additionally assessed IL-33 expression in stromal cell populations using IL-33eGFP reporter mice. Comparison between matrix fibroblasts, MPC, and preadipocyte populations showed that infection increased IL-33 expression in all subsets; however, expression was the highest in MPC, with almost 90% of cells being $IL\text{-}33eGFP^+$ (fig. S13, A and B). IL-33eGFP mean fluorescent intensity increased in MPC from infected mice, indicating increased IL-33 expression per cell (fig. S13C). Comparison of stromal cell subsets in the scRNA-seq dataset confirmed that MPC expressed *Il33* more strongly than any of the other stromal populations, in line with previous reports (fig. S14, A and B) (*7*, *8*). MPC also expressed the chemokine-encoding genes *Ccl2*, which encodes the ligand for CCR2 that is expressed on $T_H2_{RM}$ cells, and *Ccl11*, which encodes an eosinophil attractant (fig. S14B). Furthermore, MPC also expressed genes encoding ECM components and modifying enzymes, including *Fn*, *Postn*, *Ugdh*, *Pcolce2*, and *pCol1a2* (fig. S14, C and D), although expression of the latter, as well as *pCol1a2*, *pCol1a1*, *pCol3a1*, *pCol6a1*, and *Eln*, was strongest in matrix fibroblasts (fig. S14D).

Previous reports localized IL-33–producing cells to the niches around blood vessels (known as adventitia) within AT and lung tissue (*19*) and within the mesothelium of AT (*12*), which we speculate is anatomically overlapping with interstitial areas at the tissue edges (*16*). We observed that these spaces in mAT were enriched in collagen, as indicated by immunofluorescent staining for Col1 on whole tissue mounts (fig. S15). Using Pi16 and DPP4 as markers of MPC (fig. S16, cluster 2), we localized these cells primarily within interstitial spaces, including adventitia (Fig. 5K and fig. S17). Blood vessels, visualized by staining with antibodies to CD31 (fig. S18), were apparent within adventitia. MPC localization was distinct from that revealed by staining for PDGFRα, a broad stromal cell marker, which additionally showed interdigitating cells between adipocytes throughout the tissue (fig. S5C). MPC localized to interstitial spaces in mAT from both control and infected animals, but in infection, these niches appeared more densely infiltrated with cells, including with $CD4^+$ T cells (fig. S18), consistent with the observed increases in MPC and $CD4^+$ T cells during

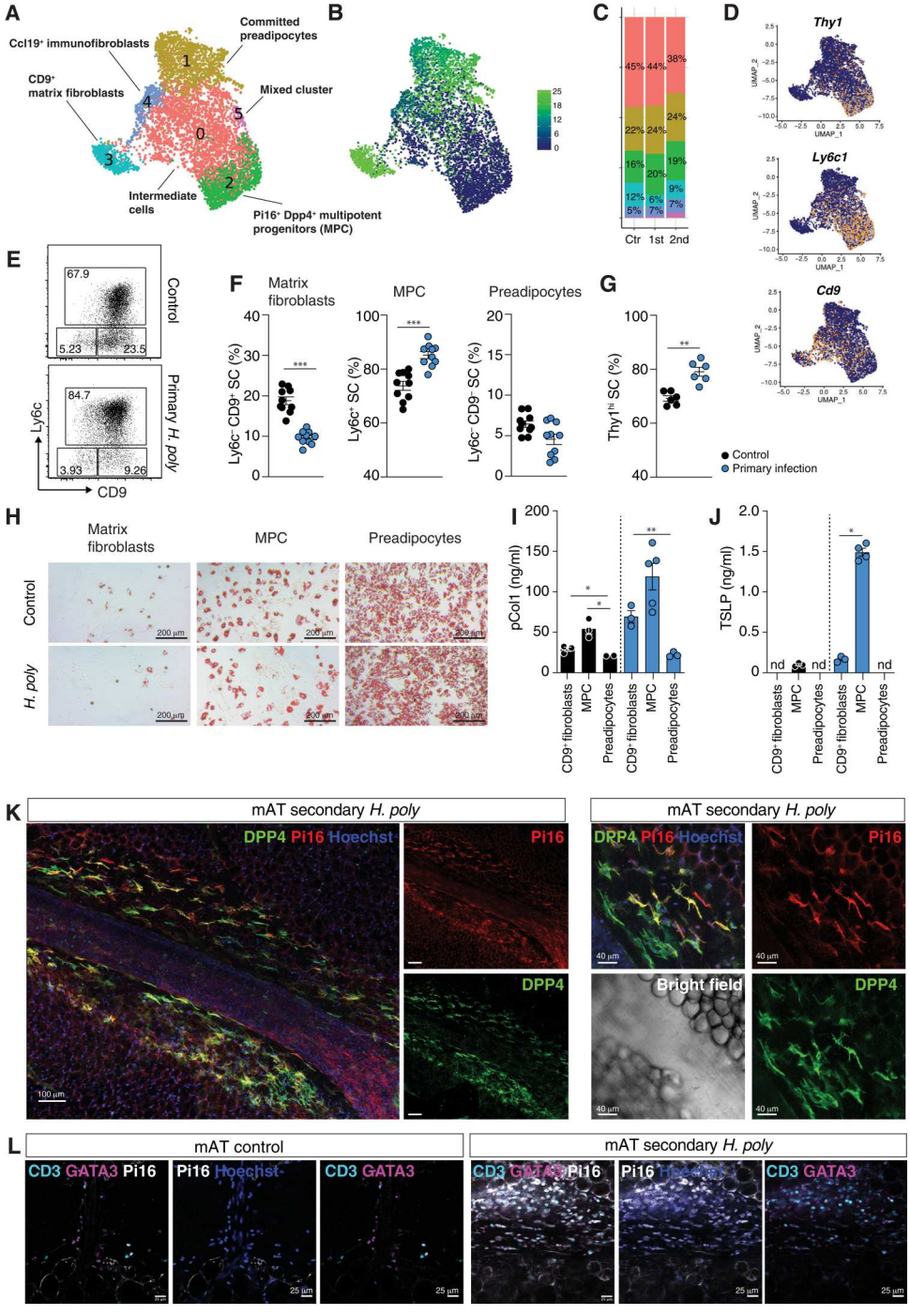


**Fig. 5. The mAT interstitial MPC population expands during infection.** (**A**) UMAP of mAT stromal cells from uninfected (control) mice (2457 cells) and mice with primary (2640 cells) or secondary (962 cells) *H. polygyrus* infections. One mouse per condition. Unsupervised clustering distinguished six cell clusters (A); plots are color-coded according to cell cluster. Cell identities were established on the basis of expression of the following markers: C1, committed preadipocytes (expressing *Icam1*, *Apoe*, *Lpl*, *Fabp4*, and *Pparg*); C2, MPC (*Dpp4*, *Anxa3*, *Cd55*, *Pi16*, and *Dpt*); C3, CD9$^+$ profibrotic cells (*Cd9*, *Wnt6*, *Eln*, *Mgp*, *Col1a1*, and *Col15a1*); and C4, immunofibroblasts (*Cd9* and *Ccl19*). (**B**) UMAP plot as in (A), showing pseudotemporal ordering of cells, setting origin at the center of MPC (C2). (**C**) Contributions of each cluster as in (A) to a total cell pool, split by experimental condition. (**D**) UMAP plots showing expression of indicated genes. (**E** and **F**) Flow cytometry plots (E) and frequencies (F) of mAT stromal cell populations from control and infected mice: Ly6c$^+$ MPC, Ly6c$^-$ CD9$^+$ matrix fibroblasts, and Ly6c$^-$ CD9$^-$ preadipocytes (gated on CD45$^-$ CD31$^-$ PDGFRα$^+$ cells). (**G**) Frequencies of Thy1$^{hi}$ mAT stromal cells in control and infected mice (gated on CD45$^-$ CD31$^-$ PDGFRα$^+$ cells). (**H**). mAT stromal cells were sorted into Ly6c$^+$ MPC, Ly6c$^-$ CD9$^+$ matrix fibroblasts, and Ly6c$^-$ CD9$^-$ preadipocytes and cultured in adipogenic conditions (see Materials and Methods). Representative images on day 6 showing lipid droplet accumulation (red staining). (**I** and **J**) pCol1 (I) and TSLP (J) production measured in supernatants from overnight culture of cells sorted as in (H). (**K**) Whole-mount immunofluorescent images of mAT from secondary infection stained for DPP4, Pi16, and nuclear staining (Hoechst). (**L**) Whole-mount immunofluorescent images of mAT from control or secondary infection stained for Pi16, CD3, GATA3, and nuclear staining (Hoechst). Data combined from two experiments (F), representative of two (G and I to L), or from one experiment (A to D). Symbols represent biological (F to G) or technical (I and J) replicates. Mean ± SEM. *$P \leq 0.05$, **$P \leq 0.01$, and ***$P \leq 0.001$. Data were analyzed by one-way unpaired ANOVA with Bonferroni's multiple comparison posttest (I), two-tailed unpaired *t* test (J), or Mann-Whitney test (F and G).

infection (Fig. 2F and fig. S12C). We found mAT adventitia to be heavily infiltrated by GATA3$^+$ $T_H2$ cells during infection, where $T_H2$ cells could be seen forming aggregates with MPC at the edges of this interstitial space (Fig. 5L and fig. S19A). Last, using IL-33eGFP reporter mice, we found DPP4$^+$ IL-33$^+$ stromal cells in proximity to CD4$^+$ T cells in the mAT interstitium during infection (fig. S19B).

Using a complementary immunohistochemistry approach on tissue sections, with CD55 as a marker for MPC (fig. S16, cluster 2), we confirmed that CD55$^+$ MPC localized to interstitial spaces, which often connected with fat-associated lymphoid clusters and were more apparent in infected mice (Fig. 6A). CD55$^+$ cells were also detectable in lymphoid clusters (Fig. 6A). Interstitial areas were clearly marked by dense collagen networks, as shown by Masson's trichrome staining (Fig. 6B), providing a context for our observation that pCol1 secretion by MPC was increased during infection (Fig. 5I). Immunohistochemistry additionally revealed details of mAT interactions with the intestine, showing that in control mice, a clear line of distinction, marked by CD55$^+$ cells, was maintained at contact points between the two tissues (Fig. 6C

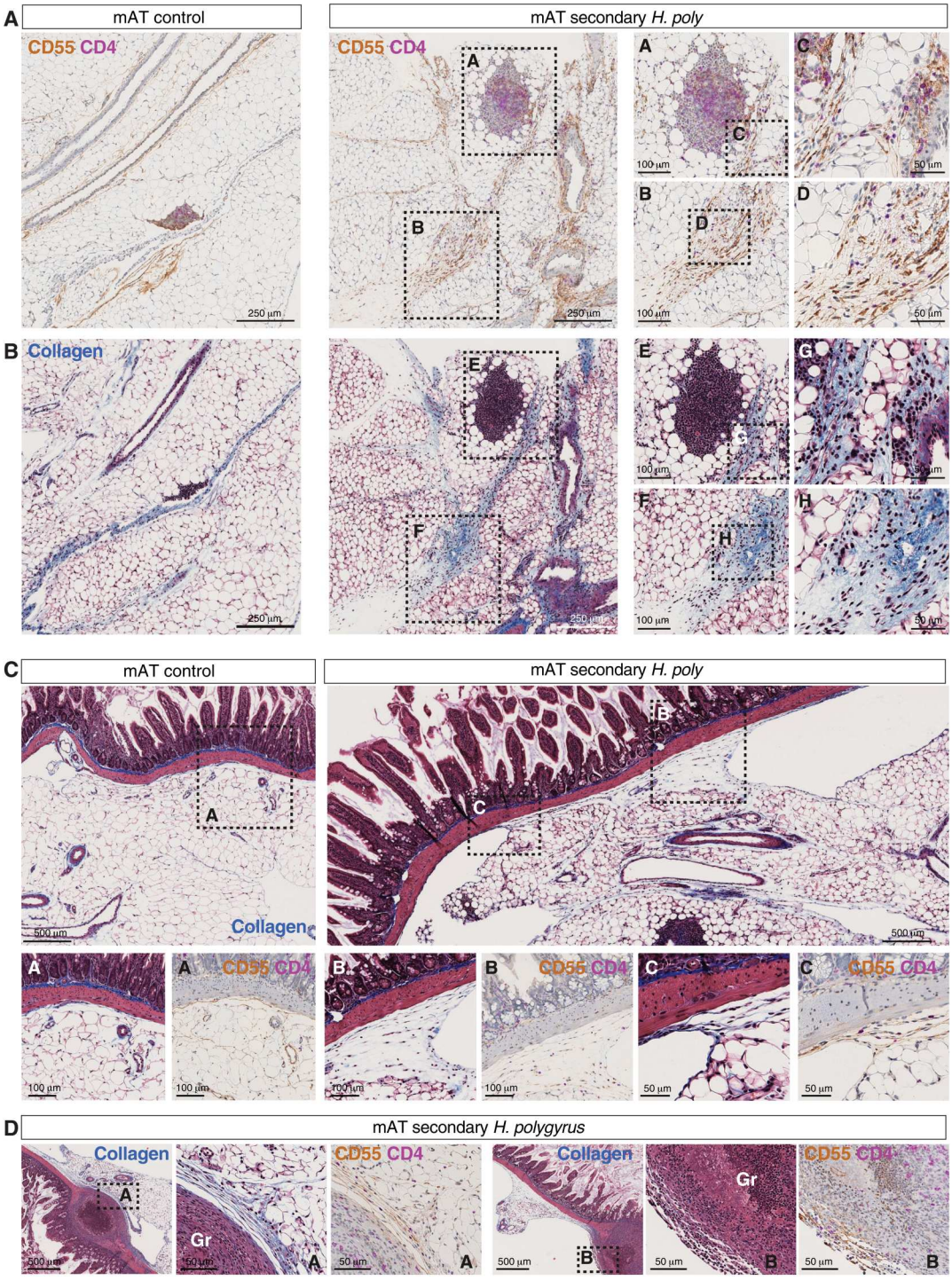


**Fig. 6. MPC and $T_H2$ cells colocalize to collagen-rich interstitial spaces in mAT during infection.** (**A** and **B**) mAT sections from uninfected (control) mice and mice with a secondary *H. polygyrus* infection. Multiplex immunohistochemistry staining for CD55/brown and CD4/purple (A) and corresponding images stained with Masson's trichrome (collagen/blue) (B). (**C** and **D**) Masson's trichrome staining and corresponding images stained for CD55 and CD4 showing interface between mAT and small intestine in control and infected mice. Squares highlight the areas shown with a higher magnification in neighboring panels. Data representative of two experiments with one or two mice per experiment (A to D). Gr, granuloma.

and fig. S20A). These areas were free of $CD4^+$ T cells (Fig. 6C and fig. S20A). During infection, however, they were often marked by adipocyte-free tissue enriched with collagen, within which $CD4^+$ T cells and $CD55^+$ MPC were numerous and interspersed (Fig. 6C and fig. S20, A and B). This was also true at the contact points with the intestinal granulomas (Fig. 6D), together indicating that interstitial tissue expands at the mAT/intestine interface during infection. Moreover, continuity of $CD55^+$ MPC-infiltrated areas between mLN, mAT, and intestine was apparent (fig. S20B), consistent with previous reports that interstitial spaces between organs are connected (*47*). To further explore the relatedness of these findings to the granulomatous response, we used RNA-seq to compare isolated granulomas and adjacent intestinal tissue from infected mice with intestinal tissue from uninfected mice. These data showed transcriptional signatures consistent with the presence of MPC and $T_H2$ cells (but not $T_{reg}$ or $T_H1$ cells) in the granulomas (fig. S21). Furthermore, it was apparent that expression of multiple ECM genes, including collagens, was increased in the granuloma tissue and mirrored the expression pattern observed in mAT stromal cells during infection (fig. S21; compare with Fig. 1J and fig. S14C).

Together, these results support the view that there is an infection-associated expansion of the MPC population within the ECM-rich interstitial spaces where $T_H2$ cells are also present. These areas expand at the interface of mAT and small intestine. The data further suggest that activation of MPC to make ECM, driven by stimulatory interactions with $T_H2$ cells, is involved in immunity to *H. polygyrus*.

### Activated stromal cells are critical for host-protective immunity to infection

Given that our data pointed to reciprocal interactions between $T_H2_{RM}$ cells with mAT stromal cells, we examined the role of cytokines produced by $T_H2_{RM}$ cells in mAT stromal cell activation. We focused on Areg, $TGF\beta_1$, IL-4, and IL-13 and first measured metabolic rates as a sensitive indicator of stromal cell activation. We found that Areg and $TGF\beta_1$ induced increased baseline OCR and spare respiratory capacity, whereas $TGF\beta_1$, but not Areg, induced aerobic glycolysis, evident by increased ECAR and increased lactate accumulation in stromal cell supernatants (Fig. 7, A to C, and fig. S22, A and B). In contrast, IL-4 and IL-13 alone had minimal effects on lactate production or spare respiratory capacity (fig. S22, A and B) but synergized with Areg to increase aerobic glycolysis (fig. S22C). We also found that Areg potentiated the increase in aerobic glycolysis induced by $TGF\beta_1$ (Fig. 7A and fig. S22C). These two cytokines also worked additively to promote OCR (Fig. 7, B and C). Consistent with this, they individually and additively promoted increases in cellular adenosine triphosphate (ATP) (Fig. 7D). Further, tracing incorporation of carbon from $^{13}C$-glucose into metabolic intermediates showed that incorporation into serine and glycine was significantly increased after stimulation with Areg and $TGF\beta_1$ (Fig. 7, E and F). Serine is a precursor for glycine, which is the most abundant amino acid in collagens. Thus, Areg and $TGF\beta_1$, two cytokines made by mAT $T_H2_{RM}$ cells, worked together to promote mAT stromal cell cellular metabolism, a prerequisite for these cells to assume an enhanced secretory function during infection (Fig. 1, S and T). Our data point to a role for Areg both individually and as a potentiator of the activity of other type 2 cytokines in the metabolic activation of mAT stromal cells.

Areg plays an important role in immunity to intestinal helminths (*48*, *49*). Although overexpression of Areg in white AT was reported to result in the loss of AT mass (*50*), relatively little is known about its function in AT biology. To begin to explore this, we examined the effects of Areg on mAT stromal cell activation ex vivo and found that it was unique among the $T_H2$ cytokines examined in being able to induce TSLP production (fig. S22D). Next, we examined the acute effects of Areg on mAT by directly injecting naïve mice with this cytokine. We found increased numbers of immune cells and stromal cells (fig. S22, E to G), which is broadly consistent with the effects of *H. polygyrus* infection (Fig. 1, D to F). We next generated mice that lack the Areg receptor epidermal growth factor receptor (EGFR) on stromal cells using *Pdgfra*-Cre ($Egfr^{fl/fl}$-*Pdgfra*-Cre mice); *Pdgfra* is broadly expressed in stromal cells (fig. S11E), and anti-PDGFRα was used here as part of the stromal cell sorting strategy. On the basis of our data showing an important role for Areg as a potentiator of stromal cell activation in response to IL-4, IL-13, and $TGF\beta_1$ (Fig. 7, A to F, and fig. S22C), we reasoned that stromal cells that could not respond to Areg would be compromised in their ability to respond fully to other cytokines made by mAT $T_H2_{RM}$ cells. Consistent with a role for Areg in modulating mAT, we found fewer stromal cells and immune cells in the mAT of $Egfr^{fl/fl}$-*Pdgfra*-Cre mice than in control mice (Fig. 7, G and I). Further, EGFR-deficient mAT stromal cells exhibited diminished responsiveness to Areg ex vivo, failing to become metabolically activated in response to this cytokine, and making less TSLP, confirming that major Areg effects on stromal cells are mediated through EGFR (fig. S22, H and I). Although EGFR is the receptor for Areg, it is additionally the receptor for EGF (*Egf*), heparin binding(HB)–EGF (*Hbegf*), transforming growth factor-α (*Tgfa*), and betacellulin (BTC), but Areg was the most expressed EGFR ligand in the mAT stromal vascular fraction during infection (fig. S23, A and B), and in this setting, $T_H2$ cells were a major source of this cytokine (fig. S7L).

To gain insight into the role of EGFR in mAT stromal cell biology during infection, we performed RNA-seq on mAT stromal cells isolated from $Egfr^{fl/fl}$-*Pdgfra*-Cre mice. We confirmed that *Egfr* expression was decreased in stromal cells from $Egfr^{fl/fl}$-*Pdgfra*-Cre mice compared with $Egfr^{fl/fl}$ controls (Fig. 7J). Lack of EGFR resulted in reduced expression of genes characteristic of MPC, including *Dpp4* and *Cd55*, and the concomitant up-regulation of genes that mark committed subsets (e.g., *Apoe*) (Fig. 7J) (*16*, *17*). Moreover, EGFR-deficient mAT stromal cells from infected mice produced less TSLP and pCol1 ex vivo than did stromal cells from infected controls (Fig. 7K and fig. S23C), and $Egfr^{fl/fl}$-*Pdgfra*-Cre mice had fewer $T_H2$ cells in mAT (fig. S23, D to F) and were more susceptible to *H. polygyrus* infection (Fig. 7, L and M). In contrast, deletion of EGFR in mature adipocytes in $Egfr^{fl/fl}$-*Adipoq*-Cre mice had no effect on susceptibility to *H. polygyrus* (fig. S23, G and H). Together, these data provide an example of how a $T_H2$-derived cytokine can influence mAT stromal cells and underscore the role of Areg through EGFR signaling for the maintenance of MPC and immunity against an intestinal parasite.

## DISCUSSION

Here, we showed that the mAT response to an enteric parasitic infection was marked by coordinated, interactional changes in the immune and stromal compartments. A population of $T_H2_{RM}$ cells

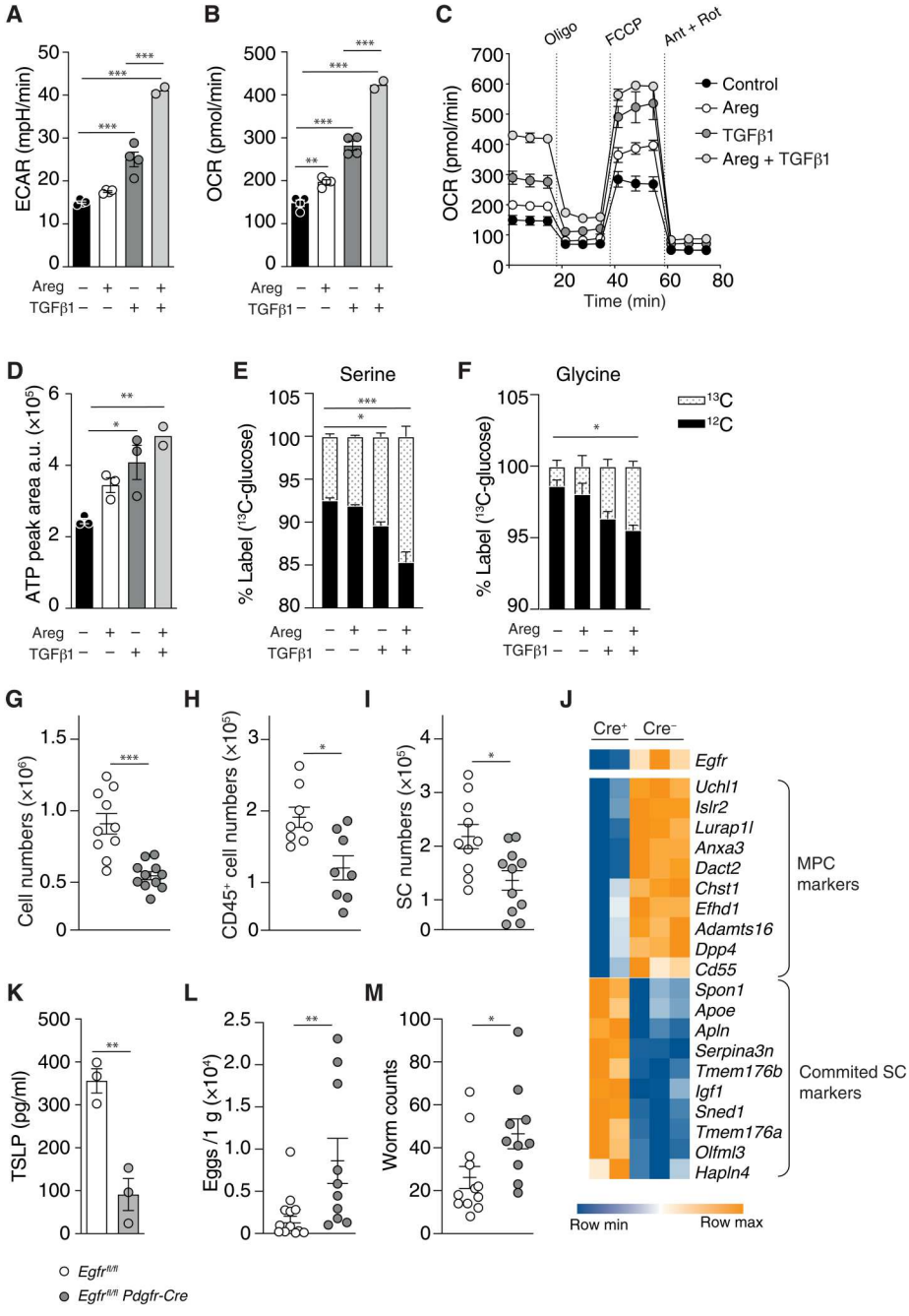


**Fig. 7. T cell cytokine-driven activation of stromal cells is important for immunity to *H. polygyrus*.** (**A** to **C**) Purified mAT stromal cells were cultured in adipogenic conditions for 3 days in the presence of indicated cytokines; baseline ECAR (A), baseline OCR (B), and OCR at baseline and after sequential addition of oligomycin (Oligo), FCCP, and rotenone/antimycin (Rot/Ant) (C, $n = 2$ to 4). (**D** to **F**) Purified mAT stromal cells were cultured in adipogenic conditions for 3 days and, during the final 6 hours, $^{12}$C-glucose was exchanged for $^{13}$C-glucose. Isotopologue distribution was assessed by targeted mass spectrometry: ATP pools (D), serine (E), and glycine (F) plotted to show fractional contributions from newly metabolized $^{13}$C or remaining $^{12}$C glucose carbons ($n = 2$ to 3). (**G** to **I**) Count of stromal vascular fraction cells (G), immune cells (CD45$^+$ CD31$^-$ cells) (H), and stromal cells (CD45$^-$ CD31$^-$ PDGFRα$^+$) (I) in mAT of *Egfr*$^{fl/fl}$ and *Egfr*$^{fl/fl}$-*Pdgfra*-Cre mice. (**J**) Expression of selected genes that mark MPC and committed stromal cells, measured by RNA-seq of sorted mAT CD31$^-$ CD45$^-$ PDGFRα$^+$ stromal cells from infected *Egfr*$^{fl/fl}$ and *Egfr*$^{fl/fl}$-*Pdgfra*-Cre mice. Each column represents stromal cells from an individual mouse. (**K**) Isolated mAT stromal cells from infected *Egfr*$^{fl/fl}$ and *Egfr*$^{fl/fl}$-*Pdgfra*-Cre mice were cultured overnight, and TSLP levels were measured in the supernatants. (**L** and **M**) Eggs in the cecum (L) and worms in the small intestine (M) were enumerated in *Egfr*$^{fl/fl}$ and *Egfr*$^{fl/fl}$-*Pdgfra*-Cre mice with primary *H. polygyrus* infections. Data combined from two (H, I, and K to M) or three (G) experiments, representative of two experiments (A to C), or from one experiment (D to F and J). Data represent biological (D to I and K to M) or technical (A to C) replicates. Mean ± SEM. $*P \leq 0.05$, $**P \leq 0.01$, and $***P \leq 0.001$. Data were analyzed by one-way unpaired ANOVA with Bonferroni's multiple comparison posttest (A to C, E, and F), two-tailed unpaired *t* test (K), or Mann-Whitney test (G to I, L, and M).

expanded and permanently dominated the mAT lymphocyte niche. This $T_H2_{RM}$ population, in response to signals from stromal cells, produced activating cytokines that drove the functional reprogramming of the stroma that was important for resistance to infection.

Pathways of adipocyte stromal cell differentiation are defined in detail, but how these are modulated by physiological perturbations has mostly been studied in the context of obesity (*13*, *16*, *18*, *43*). We found that the $T_H2$ response associated with *H. polygyrus* infection had a significant impact on the composition of mAT stromal cell populations. This was characterized by a shift toward *Dpp4*$^+$ *Pi16*$^+$ *CD55*$^+$ MPC, which became the primary producers of cytokines and collagen and which had the ability to support $T_H2_{RM}$ activation and survival. *Dpp4*$^+$ *Pi16*$^+$ stromal progenitors are a universal reservoir population containing cells capable of giving rise to differentiated fibroblast subsets (*17*) and adipocytes (*16*, *18*). These cells are localized to interstitial tissue, which is a fibroelastic connective tissue that envelops internal organs and blood vessels (where it is called the adventitia) and which is also found beneath the skin (where it is referred to as the fascia) (*51*). Evidence suggests continuity of interstitial tissue within and between organs, possibly providing a pathway for cell and antigen movement that is alternative to vascular or lymphatic routes (*47*, *52*, *53*).

Studies in the skin show that mobilization of cells within the fascia is critical for wound healing (*54*). Recent work exploring changes in stromal cells and immune cells in the skin after transient postnatal $T_{reg}$ cell depletion identifies the accumulation of stromal cells with the characteristics of MPC in fibrous bands in the skin and the parallel accumulation of persistent $T_H2$ cells in the tissue, both of which associate with skin healing (*20*). The authors refer to these stromal cells as $T_H2$-interacting fascial fibroblasts, linking previous evidence that cells with MPC characteristics are specialized for supporting type 2 immune responses (*19*, *55*) with the localization of IL-33–producing cells to the adventitia and fascia (*13*, *16*, *17*, *19*). Our findings are consistent with these reports and together point to a general phenomenon in which expansion and activation of the MPC population is a hallmark of the physiological response to type 2 inflammation that is shared across tissues. We speculate that the benefit of such a response is linked to the plasticity of this stromal cell subset to assume new supportive functions in response to signals received from the immune system. In the case of infection with *H. polygyrus*, we favor the view that the accumulation of MPC reflects a block in their differentiation into committed preadipocytes, a process that could contribute to the reduction in AT mass associated with infection. Alternative explanations for the accumulation of MPC are that adipocytes dedifferentiate into these cells during infection (*56*, *57*) or that cells of this type migrate into mAT from other tissues. The reported continuity of the reticular interstitium between tissues (*47*) would provide a pathway for MPC to move in this way. This anatomical link provides a possible connection between immunological events in the mAT and adjacent mLN and intestine, suggesting that infection-driven activation of interstitial niches could facilitate cell migration to support immunity. Our imaging results, which showed the presence of MPC at the interface between the mAT and the small intestine, are consistent with this being the case. Thus, the interstitial space within mAT is emerging as a specialized location for interactions between immune cells and stromal cells.

Similarly to immune cells, stromal cells can engage different metabolic modules depending on their differentiation stage and function. ECM remodeling regulates glucose metabolism (*58*), but how these cells adapt metabolically to inflammation is not well understood (*59*). We found that metabolic activation of mAT stromal cells was a hallmark of the response to *H. polygyrus* infection and critical for increased ECM production. Metabolic activation in stromal cells resulted in increased incorporation of glucose into serine and glycine and in increased ATP levels. This is consistent with a requirement for glycine to support increased synthesis of collagens in which ~30% of amino acids are glycine and for increased cellular ATP to meet the energetic demands of protein translation in cells that have assumed a highly biosynthetic role, producing ECM, cytokines, and chemokines for export after stimulation by $T_H2$-derived cytokines. As for collagen synthesis and cytokine production, metabolic changes were more pronounced in mAT stromal cells from mice responding to a secondary versus primary infection. This raises the possibility that stromal cells may exhibit innate memory analogous to that described for innate immune cells, in which primary exposure to a stimulus results in metabolism-dependent epigenetic changes around responsive genes that allow the cells to respond more strongly upon secondary stimulation (*60*, *61*). Alternatively, this may reflect ongoing effects of stronger in vivo stimulation related to larger numbers of $T_H2_{RM}$ cells in the mAT. The presence of $T_H2_{RM}$ cells in gAT from infected mice, in the absence of activated stromal cells, and the dependence of stromal cell activation on $T_H2$ cells suggest that the activation status of $T_H2_{RM}$ cells is dictated by the anatomical proximity to the site of infection and related to stromal cell activation.

mAT activation in infected mice shares some features, including the activation of stromal cells to make Col1A1, with the creeping fibrotic mAT of Crohn′s disease. Creeping fat serves to prevent the systemic spread of intestinal bacteria, which translocate across the gut wall due to loss of epithelial integrity associated with Crohn′s disease (*62*). *H. polygyrus* are not thought to penetrate the gut wall, but on the basis of the creeping fat model, we speculate that increased collagen deposition within mAT may reflect a defensive process aimed at increasing the strength and resilience of the intestine and its associated vasculature to minimize the possibility and consequences of perforation. Despite the presence within the mAT of CD9$^+$ matrix fibroblasts, which strongly expressed collagen genes, the MPC were the main source of pCol1 protein during infection and also appeared to be the dominant producers of fibrinogen (Fn1), fibrillin (Fbn1), and uridine diphosphate–glucose 6-dehydrogenase (Udgh), which together are critical components of the ECM. Increased mechanical stiffness of the ECM can potentiate cell migration (*63*, *64*) and therefore may also play a role in $T_H2$ cell and other immune cell movement into and through the interstitial spaces. Moreover, it can influence stem cell fate determination (*65*), so it is feasible that the changes in ECM during infection observed here could contribute to the accumulation of MPC. Perhaps related to this, MPC identity is maintained by TGF$\beta_1$ (*16*), and in this context, it is notable that mAT $T_H2_{RM}$ cells produced this cytokine.

Persistence of a large population of mAT $T_H2_{RM}$ cells almost a year after clearance of infection was notable and consistent with reports of the longevity of lung $T_H2_{RM}$ cells (*66*). $T_H2_{RM}$ cells within mAT expressed *Arg1*, *Nmur1*, and *Calca*, which have previously been considered to be primarily expressed by ILC2 (*67*–*70*). This pattern of gene expression, together with their ability to become activated directly by cytokines, supports the view that innate reprogramming of $T_H2$ cells is an integral part of terminal

differentiation driven by exposure to tissue-derived cytokine such as TSLP and IL-33 (*34*, *40*, *71*). Similarities between mAT $T_H2$ cells and mAT ILC2 indicate that tissue residency is promoting convergent transcriptional patterns in different type 2 immune cells, an idea already seen with similarities between $T_H2$ cells and ILC2 in lungs and small intestine (*34*). In this context, it is of interest that interactions between ILC2 and stromal cells, like those shown here for $T_H2$ cells and stromal cells, also occur within the adventitia (*12*, *19*).

In addition to classic type 2 cytokines, mAT $T_H2_{RM}$ cells also produced Areg, a cytokine previously implicated in immunity to intestinal helminths (*48*, *49*). Areg produced by $T_{reg}$ cells has also been linked with tissue repair (*72*), but our data indicate that during and after *H. polygyrus* infection such a reparative role could be falling largely to the persistent $T_H2_{RM}$ population. Relatively little is known of roles for Areg and EGFR signaling in AT physiology. However, previous work indicated that autocrine signaling via EGFR in $T_H2$ cells is important for immunity to intestinal nematodes, because coordinated signaling through EGFR and the IL-33 receptor is essential for $T_H2$ cells to make IL-13 (*49*). We observed that in addition to this pathway, Areg was able to drive TSLP production by mAT stromal cells. This cross-talk between Areg and TSLP production could stabilize the lymphoid niche within the tissue and therefore have implications for the persistence of $T_H2_{RM}$ cells in mAT. The fact that Areg can release $TGF\beta_1$ from latent $TGF\beta_1$ through integrin-$\alpha_v$ activation (*73*) indicates that polyfunctional $T_H2_{RM}$ cells capable of making both cytokines may be particularly potent sources of active $TGF\beta_1$. In our experiments, synergy between Areg and $TGF\beta_1$ was apparent in vitro, where Areg was able to prime stromal cells for enhanced metabolic responses to $TGF\beta_1$. This is consistent with previous reports of cross-talk between EGFR- and $TGF\beta_1$-induced events in the development of kidney fibrosis (*74*). Deletion of *Egfr* in stromal cells emphasized the importance of Areg signaling for modulating stromal vascular fraction cellularity in mAT and for protective immunity against an enteric infection. Our results support an emerging view of EGFR signaling in stromal cells providing a critical component of tissue immunity against helminth infection. Although our experiments did not allow identification of stromal cells specifically in mAT as critical for immunity, we found MPC at the interface between mAT and small intestine in what we believe are conduits between the two organs and adjacent to granulomas. This raises the possibility that these cells can directly contribute to strengthening of the intestinal wall and supporting granuloma formation.

Our findings on mAT contribute to the growing realization that AT can provide help to tissues fighting infection or recovering from wounding (*26*, *75*–*77*). These findings warrant broader consideration of the function of AT during disease. The extent to which changes in populations of resident immune cells affect the helper activity of AT has been unclear, but our findings indicate that this may be of major significance because immune cells and AT stromal cells have evolved powerful dynamic mechanisms for reciprocal activation and regulation.

## MATERIALS AND METHODS

### Study design

The objective of this study was to investigate the role of mAT remodeling that is driven by intestinal infection with *H. polygyrus* in mice. We studied changes in immune and stromal cell populations using RNA-seq and scRNA-seq technologies, flow cytometry, enzyme-linked immunosorbent assay (ELISA)–based measurements, metabolic profiling, and immunofluorescence and immunohistology imaging. Studies in which primary *H. polygyrus* infection was analyzed had an end point between days 11 and 14, which permitted the assessment of adult worm burden and adaptive immune responses. To study memory responses, we repeated *H. polygyrus* infection 5 weeks after the clearance of initial infection and analysis was again performed between days 11 and 14. We used age- and sex-matched mice. Group sizes were determined on the basis of experimental purposes using previous experience or estimated on the basis of preliminary data. This study was not blinded. Sampling and experimental replicates are indicated in the figure legends.

### Mouse models

C57BL/6J (the Jackson Laboratory: 000664), Balb/cJ (the Jackson Laboratory: 000651), *Cd4*-Cre (the Jackson Laboratory: 022071), *Pdgfra*-Cre (the Jackson Laboratory:013148), *Il4*eGFP *Foxp3*RFP *Il10*Bit [generated by crossing $Il4^{tm1Lky}$ (*78*), $Foxp3^{tm1Flv}$ (*79*), and Tg(Il10-Thy1a) (*80*) mice], $Il4ra^{tm2Fbb}$ (IL-4Rfl/fl) (*81*), $Egfr^{tm1Dwt}$ (EGFRfl/fl) (*82*), B6(129S4)-$Il33^{tm1.1Bryc}$/J (the Jackson Laboratory: 030619), and B6;FVB-Tg(Adipoq-cre)1Evdr/J (the Jackson Laboratory: 028020) mice were used. Mice were maintained at the Washington University School of Medicine in St. Louis, the Max Planck Institute for Immunobiology and Epigenetics, or the Bloomberg-Kimmel Institute for Cancer Immunotherapy at Johns Hopkins. All corresponding animal protocols were approved by the animal care committee of the Regierungspraesidium Freiburg, the Animal Care and Use Committee (ACUC) of Washington University in St. Louis, or the ACUC of Johns Hopkins University. Mice were bred under specific pathogen–free standards. Animals used for tissue harvest or experimental procedures were aged between 7 and 12 weeks at the start of the experiment and were age- and sex-matched. Both female and male mice were used in the study.

### Experimental infections and interventions

*H. polygyrus bakeri* L3-stage larvae were prepared at the U.S. Department of Agriculture (Beltsville, USA) (*83*). For *H. polygyrus* infection, mice were each gavaged with 200 L3-stage larvae in phosphate-buffered saline (PBS). For primary infection, mice were left for 11 to 14 days before being euthanized or treated with the anthelminthic pyrantel pamoate (1 mg per mouse). For secondary infection, mice were infected at 5 weeks after treatment and euthanized 11 to 14 days later. For *H. polygyrus* egg and adult worm counts, small intestines were removed, opened longitudinally, and placed into a mesh cloth on top of a 50-ml tube filled with PBS for 3 to 4 hours in a 37°C water bath. Adult parasites dropped through the mesh into the tube and were recovered for counting on a dissecting microscope. Parasite eggs were isolated by floatation on saturated sodium chloride from cecal contents collected from individual mice and counted under a microscope. For $CD4^+$ T cell depletion, mice were infected; treated; and, 5 weeks later, injected with anti-CD4 monoclonal antibody (mAb) (500 μg per mouse intraperitoneally per injection; clone GK1.5, Bio X Cell) 1 day before secondary infection and then again at day 6 after infection. Mice were euthanized on day 11 of secondary infection. For IL-7Rα blockade, mice were infected and treated and injected with anti–IL-7Rα mAb (500 μg per mouse intraperitoneally per injection; clone A7R34, Bio

X Cell) on days 3 and 9 after treatment and euthanized on day 12 after treatment. For treatment with FTY720 (Enzo, BML-SL233-0005), mice were infected and treated and, 5 weeks later, injected with FTY720 every second day, starting from 1 day before secondary infection (six injections in total, 10 μg per mouse intraperitoneally per injection). Mice were euthanized on day 11 of secondary infection. For Areg (R&D Systems, 989-AR) treatment, naïve mice were injected three times with Areg (10 μg per mouse intraperitoneally) on days 0, 3, and 6 and were euthanized on day 9. For IL-33 (BioLegend,580504) treatment, naïve mice were injected three times on three consecutive days with IL-33 (1 μg per mouse intraperitoneally) and euthanized on day 9. For the magnetic resonance imaging (MRI), the EchoMRI 3-in-1 Body Composition Analyzer was used according to the manufacturer's instructions. To assess food intake, mice were housed three per cage and chow consumption per day was estimated on the basis of the weight of chow remaining in the food hopper and divided by the number of mice in the cage to obtain chow consumption per day per mouse measurement. High-fat diet experiments used chow containing 60% fat (Research Diets, D12492i).

### Cell isolation and culture

Stromal cells and immune cells were isolated from tissues obtained from euthanized and PBS-perfused animals. For isolation from mAT, gAT, and small intestine lamina propria (SI LP), enzymatic tissue digestion was performed. To purify $T_H2$ cells (TCRβ$^+$ CD4$^+$ IL4-eGFP$^+$ FOXP3-RFP$^-$), non-$T_H2$/non-$T_{reg}$ cells (CD45$^+$ TCRβ$^+$ CD4$^+$ IL4-eGFP$^-$ FOXP3-RFP$^-$), and stromal cell subpopulations (based on Ly6c and CD9 expression), we isolated cells via FACS, excluding dead cells and doublets. Total mAT and gAT stromal cells were isolated using the Adipose Tissue Progenitor Isolation Kit (Miltenyi Biotec, 130-106-639). Stromal cells were plated at $2 \times 10^5$ to $4 \times 10^5$ cells per well and cultured overnight. Supernatants were collected, and cytokines or pCol1 was measured by ELISA. In experiments where effects of cytokines on stromal cell biology or adipogenic potential of mAT stromal cell subpopulations were assessed, adipogenic factors were added to mimic AT conditions. For details of cell isolation and culture, see Supplementary Materials and Methods.

### Flow cytometry

For analysis of intracellular cytokine production, cells were restimulated for 4 hours with phorbol 12-myristate 13- acetate (0.1 μg/ml), ionomycin (1 μg/ml), and brefeldin A (10 μg/ml). Cells were surface-stained with mAbs diluted in PBS/0.1% bovine serum albumin (BSA) and Fc-block (BioLegend) for 30 min on ice. Fixable Viability Dye (eBioscience) was added to allow the exclusion of dead cells. For intracellular staining, cells were fixed and permeabilized using the FOXP3/transcription factor staining kit (eBioscience). The list of antibodies and more details on the flow cytometry protocols can be found in Supplementary Materials and Methods.

### Microscopy

Hematoxylin and eosin (H&E), Masson's trichrome, or CD55/CD4 multiplex immunostaining were performed on formalin-fixed, paraffin-embedded tissue sections. Images were acquired using a Zeiss Axio Imager Apotome or Hamamatsu NanoZoomer S210 Digital slide scanner.

For immunofluorescent whole-mount staining of CD3, CD4, CD31, DPP4, Pi16, GATA3, perilipin1, PDGFRα, collagen 1, and IL-33, mAT samples were formalin-fixed, permeabilized in 1% Triton X-100 in PBS (Sigma-Aldrich), blocked with 2.5% BSA and 0.5% Triton X-100 in PBS, and incubated with primary antibodies, followed by staining with secondary antibodies and nuclear staining (Hoechst 33342). Samples were mounted with ProLong Diamond Antifade Mountant (Thermo Fisher Scientific). Confocal images were acquired using a Zeiss spinning disk confocal microscope equipped with a Photometrics Prime BSI camera and Apochromat objectives or with a Zeiss Axio Observer inverted microscope with a LSM800 confocal module. For details, see Supplementary Materials and Methods.

### RNA sequencing

The Ambion's RNAqueous-Micro Kit (catalog no. 1931) or Qiagen RNeasy Kit (catalog no. 75144) was used for bulk RNA isolation from sort-purified PDGFRα$^+$ Sca1$^+$ stromal cells from C57BL/6J mice (Fig. 1, I and J) and PDGFRα$^+$ Sca1$^+$ stromal cells from *Egfr*$^{fl/fl}$-*Pdgfra*-Cre mice (Fig. 7J). RNA isolation from granulomas and unaffected small intestinal tissues (fig. S19) was done using oligo(dT) beads (Invitrogen). scRNA-seq of sort-purified mAT stromal vascular fraction cells was performed using the 10X Genomics Chromium Controller. scRNA-seq of sort-purified CD4$^+$ TCRβ$^+$ T cells from mLN, mAT, and small intestine lamina propria was performed using the CEL-Seq2 method (*84*) with modifications as described (*85*). Details for RNA-seq and scRNA-seq are included in Supplementary Materials and Methods.

### Metabolic profiling

OCR and ECAR were measured in XF media under basal conditions and in response to 1 μM oligomycin, 1.5 μM fluoro-carbonyl cyanide phenylhydrazone (FCCP), and 100 nM rotenone + 1 μM antimycin A using the 96-well XF or XFe Extracellular Flux Analyzer (Seahorse Bioscience). For stable isotope tracing, mAT stromal cells isolated from naïve mice were cultured in adipogenic differentiation conditions for 3 days, and during the final 6 hours, $^{12}$C-glucose was replaced with uniformly heavy-labeled $^{13}$C-glucose. Cell metabolites were extracted using 70 μl of extraction buffer (50:30:20, methanol:acetonitrile:water). Metabolite measurements were made via liquid chromatography–mass spectrometry (LC-MS) using an Agilent 1290 Infinity II ultrahigh-performance liquid chromatography (UHPLC) system in line with a Bruker Impact II QTOF operating in negative ion mode. Metabolites were quantified using AssayR (*86*) and identified by matching accurate mass and retention time to standards. For details, see Supplementary Materials and Methods.

### Quantification and statistical analysis

With the exception of scRNA-seq and RNA-seq datasets, statistical analyses were performed using Prism 7 software (GraphPad). Comparisons for two groups were calculated using rank Mann-Whitney or unpaired *t* tests. Comparisons of more than two groups were calculated using one-way ordinary unpaired analysis of variance (ANOVA) with Bonferroni's multiple comparison tests. Tests were two-sided and $\alpha = 0.05$ (95% confidence interval).

## Supplementary Materials

**This PDF file includes:**
Materials and Methods
Figs. S1 to S23
Table S1
References (*87*–*97*)

**Other Supplementary Material for this manuscript includes the following:**
Raw data

View/request a protocol for this paper from *Bio-protocol*.

## REFERENCES AND NOTES


1. J. Ordovas-Montanes, S. Beyaz, S. Rakoff-Nahoum, A. K. Shalek, Distribution and storage of inflammatory memory in barrier tissues. *Nat. Rev. Immunol.* **20**, 308–320 (2020).
2. C. E. O'Leary, C. Schneider, R. M. Locksley, Tuft cells-systemically dispersed sensory epithelia integrating immune and neural circuitry. *Annu. Rev. Immunol.* **37**, 47–72 (2019).
3. J. von Moltke, M. Pepper, Sentinels of the type 2 immune response. *Trends Immunol.* **39**, 99–111 (2018).
4. R. L. Gieseck III, M. S. Wilson, T. A. Wynn, Type 2 immunity in tissue repair and fibrosis. *Nat. Rev. Immunol.* **18**, 62–76 (2018).
5. F. Roan, K. Obata-Ninomiya, S. F. Ziegler, Epithelial cell-derived cytokines: More than just signaling the alarm. *J. Clin. Invest.* **129**, 1441–1451 (2019).
6. A. B. Molofsky, J. C. Nussbaum, H. E. Liang, S. J. Van Dyken, L. E. Cheng, A. Mohapatra, A. Chawla, R. M. Locksley, Innate lymphoid type 2 cells sustain visceral adipose tissue eosinophils and alternatively activated macrophages. *J. Exp. Med.* **210**, 535–549 (2013).
7. J. R. Brestoff, B. S. Kim, S. A. Saenz, R. R. Stine, L. A. Monticelli, G. F. Sonnenberg, J. J. Thome, D. L. Farber, K. Lutfy, P. Seale, D. Artis, Group 2 innate lymphoid cells promote beiging of white adipose tissue and limit obesity. *Nature* **519**, 242–246 (2015).
8. M. W. Lee, J. I. Odegaard, L. Mukundan, Y. F. Qiu, A. B. Molofsky, J. C. Nussbaum, K. R. Yun, R. M. Locksley, A. Chawla, Activated type 2 innate lymphoid cells regulate beige fat biogenesis. *Cell* **160**, 74–87 (2015).
9. D. Wu, A. B. Molofsky, H. E. Liang, R. R. Ricardo-Gonzalez, H. A. Jouihan, J. K. Bando, A. Chawla, R. M. Locksley, Eosinophils sustain adipose alternatively activated macrophages associated with glucose homeostasis. *Science* **332**, 243–247 (2011).
10. D. Cipolletta, M. Feuerer, A. Li, N. Kamei, J. Lee, S. E. Shoelson, C. Benoist, D. Mathis, PPAR-γ is a major driver of the accumulation and phenotype of adipose tissue $T_{reg}$ cells. *Nature* **486**, 549–553 (2012).
11. A. Vasanthakumar, K. Moro, A. Xin, Y. Liao, R. Gloury, S. Kawamoto, S. Fagarasan, L. A. Mielke, S. Afshar-Sterle, S. L. Masters, S. Nakae, H. Saito, J. M. Wentworth, P. Li, W. Liao, W. J. Leonard, G. K. Smyth, W. Shi, S. L. Nutt, S. Koyasu, A. Kallies, The transcriptional regulators IRF4, BATF, and IL-33 orchestrate development and maintenance of adipose tissue-resident regulatory T cells. *Nat. Immunol.* **16**, 276–285 (2015).
12. T. Mahlakoiv, A. L. Flamar, L. K. Johnston, S. Moriyama, G. G. Putzel, P. J. Bryce, D. Artis, Stromal cells maintain immune cell homeostasis in adipose tissue via production of interleukin-33. *Sci. Immunol.* **4**, eaax0416 (2019).
13. R. G. Spallanzani, D. Zemmour, T. Xiao, T. Jayewickreme, C. Li, P. J. Bryce, C. Benoist, D. Mathis, Distinct immunocyte-promoting and adipocyte-generating stromal components coordinate adipose tissue immune and metabolic tenors. *Sci. Immunol.* **4**, eaaw3658 (2019).
14. B. M. J. Rana, E. Jou, J. L. Barlow, N. Rodriguez-Rodriguez, J. A. Walker, C. Knox, H. E. Jolin, C. S. Hardman, M. Sivasubramaniam, A. Szeto, E. S. Cohen, I. C. Scott, M. A. Sleeman, C. I. Chidomere, S. Cruz Migoni, J. Caamano, H. F. Jorgensen, S. Carobbio, A. Vidal-Puig, A. N. J. McKenzie, A stromal cell niche sustains ILC2-mediated type-2 conditioning in adipose tissue. *J. Exp. Med.* **216**, 1999–2009 (2019).
15. D. Kolodin, N. van Panhuys, C. Li, A. M. Magnuson, D. Cipolletta, C. M. Miller, A. Wagers, R. N. Germain, C. Benoist, D. Mathis, Antigen- and cytokine-driven accumulation of regulatory T cells in visceral adipose tissue of lean mice. *Cell Metab.* **21**, 543–557 (2015).
16. D. Merrick, A. Sakers, Z. Irgebay, C. Okada, C. Calvert, M. P. Morley, I. Percec, P. Seale, Identification of a mesenchymal progenitor cell hierarchy in adipose tissue. *Science* **364**, eaav2501 (2019).
17. M. B. Buechler, R. N. Pradhan, A. T. Krishnamurty, C. Cox, A. K. Calviello, A. W. Wang, Y. A. Yang, L. Tam, R. Caothien, M. Roose-Girma, Z. Modrusan, J. R. Arron, R. Bourgon, S. Müller, S. J. Turley, Cross-tissue organization of the fibroblast lineage. *Nature* **593**, 575–579 (2021).
18. P. Cattaneo, D. Mukherjee, S. Spinozzi, L. Zhang, V. Larcher, W. B. Stallcup, H. Kataoka, J. Chen, S. Dimmeler, S. M. Evans, N. Guimaraes-Camboa, Parallel lineage-tracing studies establish fibroblasts as the prevailing in vivo adipocyte progenitor. *Cell Rep.* **30**, 571–582.e2 (2020).
19. M. W. Dahlgren, S. W. Jones, K. M. Cautivo, A. Dubinin, J. F. Ortiz-Carpena, S. Farhat, K. S. Yu, K. Lee, C. Wang, A. V. Molofsky, A. D. Tward, M. F. Krummel, T. Peng, A. B. Molofsky, Adventitial stromal cells define group 2 innate lymphoid cell tissue niches. *Immunity* **50**, 707–722.e6 (2019).
20. I. C. Boothby, M. J. Kinet, D. P. Boda, E. Y. Kwan, S. Clancy, J. N. Cohen, I. Habrylo, M. M. Lowe, M. Pauli, A. E. Yates, J. D. Chan, H. W. Harris, I. M. Neuhaus, T. H. McCalmont, A. B. Molofsky, M. D. Rosenblum, Early-life inflammation primes a T helper 2 cell-fibroblast niche in skin. *Nature* **599**, 667–672 (2021).
21. M. D. Taylor, N. van der Werf, R. M. Maizels, T cells in helminth infection: The regulators and the regulated. *Trends Immunol.* **33**, 181–189 (2012).
22. S. Obi, C. Shimokawa, M. Katsuura, A. Olia, T. Imai, K. Suzue, H. Hisaeda, IL-33 is essential to prevent high-fat diet-induced obesity in mice infected with an intestinal helminth. *Parasite Immunol.* **42**, e12700 (2020).
23. C. W. Su, C. Y. Chen, Y. Li, S. R. Long, W. Massey, D. V. Kumar, W. A. Walker, H. N. Shi, Helminth infection protects against high fat diet-induced obesity via induction of alternatively activated macrophages. *Sci. Rep.* **8**, 4607 (2018).
24. L. Hussaarts, N. García-Tardón, L. van Beek, M. M. Heemskerk, S. Haeberlein, G. C. van der Zon, A. Ozir-Fazalalikhan, J. F. Berbée, K. W. van Dijk, V. van Harmelen, M. Yazdanbakhsh, B. Guigas, Chronic helminth infection and helminth-derived egg antigens promote adipose tissue M2 macrophages and improve insulin sensitivity in obese mice. *FASEB J.* **29**, 3027–3039 (2015).
25. G. Caputa, M. Matsushita, D. E. Sanin, A. M. Kabat, J. Edwards-Hicks, K. M. Grzes, R. Pohlmeyer, M. A. Stanczak, A. Castoldi, J. Cupovic, A. J. Forde, P. Apostolova, M. Seidl, N. van Teijlingen Bakker, M. Villa, F. Baixauli, A. Quintana, A. Hackl, L. Flachsmann, F. Hässler, J. D. Curtis, A. E. Patterson, P. Henneke, E. L. Pearce, E. J. Pearce, Intracellular infection and immune system cues rewire adipocytes to acquire immune function. *Cell Metab.* **34**, 747–760.e6 (2022).
26. S. J. Han, A. Glatman Zaretsky, V. Andrade-Oliveira, N. Collins, A. Dzutsev, J. Shaik, D. Morais da Fonseca, O. J. Harrison, S. Tamoutounour, A. L. Byrd, M. Smelkinson, N. Bouladoux, J. B. Bliska, J. M. Brenchley, I. E. Brodsky, Y. Belkaid, White adipose tissue is a reservoir for memory T cells and promotes protective memory responses to infection. *Immunity* **47**, 1154–1168.e6 (2017).
27. R. K. Zwick, C. F. Guerrero-Juarez, V. Horsley, M. V. Plikus, Anatomical, physiological, and functional diversity of adipose tissue. *Cell Metab.* **27**, 68–83 (2018).
28. R. Nigdelioglu, R. B. Hamanaka, A. Y. Meliton, E. O'Leary, L. J. Witt, T. Cho, K. Sun, C. Bonham, D. Wu, P. S. Woods, A. N. Husain, D. Wolfgeher, N. O. Dulin, N. S. Chandel, G. M. Mutlu, Transforming growth factor (TGF)-β promotes de novo serine synthesis for collagen production. *J. Biol. Chem.* **291**, 27239–27251 (2016).
29. S. Schwörer, M. Berisa, S. Violante, W. Qin, J. Zhu, R. C. Hendrickson, J. R. Cross, C. B. Thompson, Proline biosynthesis is a vent for TGFβ-induced mitochondrial redox stress. *EMBO J.* **39**, e103334 (2020).
30. X. Zhao, P. Psarianos, L. S. Ghoraie, K. Yip, D. Goldstein, R. Gilbert, I. Witterick, H. Pang, A. Hussain, J. H. Lee, J. Williams, S. V. Bratman, L. Ailles, B. Haibe-Kains, F.-F. Liu, Metabolic regulation of dermal fibroblasts contributes to skin extracellular matrix homeostasis and fibrosis. *Nat. Metab.* **1**, 147–157 (2019).
31. G. J. van der Windt, B. Everts, C. H. Chang, J. D. Curtis, T. C. Freitas, E. Amiel, E. J. Pearce, E. L. Pearce, Mitochondrial respiratory capacity is a critical regulator of $CD8^+$ T cell memory development. *Immunity* **36**, 68–78 (2012).
32. C. Bénézech, N. T. Luu, J. A. Walker, A. A. Kruglov, Y. Loo, K. Nakamura, Y. Zhang, S. Nayar, L. H. Jones, A. Flores-Langarica, A. McIntosh, J. Marshall, F. Barone, G. Besra, K. Miles, J. E. Allen, M. Gray, G. Kollias, A. F. Cunningham, D. R. Withers, K. M. Toellner, N. D. Jones, M. Veldhoen, S. A. Nedospasov, A. N. J. McKenzie, J. H. Caamano, Inflammation-induced formation of fat-associated lymphoid clusters. *Nat. Immunol.* **16**, 819–828 (2015).
33. K. Moro, T. Yamada, M. Tanabe, T. Takeuchi, T. Ikawa, H. Kawamoto, J. Furusawa, M. Ohtani, H. Fujii, S. Koyasu, Innate production of $T_H2$ cytokines by adipose tissue-associated c-$Kit^+Sca\text{-}1^+$ lymphoid cells. *Nature* **463**, 540–544 (2010).
34. S. J. Van Dyken, J. C. Nussbaum, J. Lee, A. B. Molofsky, H. E. Liang, J. L. Pollack, R. E. Gate, G. E. Haliburton, C. J. Ye, A. Marson, D. J. Erle, R. M. Locksley, A tissue checkpoint regulates type 2 immunity. *Nat. Immunol.* **17**, 1381–1387 (2016).
35. D. Grun, Revealing dynamics of gene expression variability in cell state space. *Nat. Methods* **17**, 45–49 (2020).
36. S. Steinfelder, S. Rausch, D. Michael, A. A. Kühl, S. Hartmann, Intestinal helminth infection induces highly functional resident memory $CD4^+$ T cells in mice. *Eur. J. Immunol.* **47**, 353–363 (2017).

37. R. R. Ricardo-Gonzalez, S. J. Van Dyken, C. Schneider, J. Lee, J. C. Nussbaum, H. E. Liang, D. Vaka, W. L. Eckalbar, A. B. Molofsky, D. J. Erle, R. M. Locksley, Tissue signals imprint ILC2 identity with anticipatory function. *Nat. Immunol.* **19**, 1093–1099 (2018).
38. D. Masopust, A. G. Soerens, Tissue-resident T cells and other resident leukocytes. *Annu. Rev. Immunol.* **37**, 521–546 (2019).
39. M. Kitajima, H. C. Lee, T. Nakayama, S. F. Ziegler, TSLP enhances the function of helper type 2 cells. *Eur. J. Immunol.* **41**, 1862–1871 (2011).
40. M. Peine, R. M. Marek, M. Löhning, IL-33 in T cell differentiation, function, and immune homeostasis. *Trends Immunol.* **37**, 321–333 (2016).
41. J. Corren, S. F. Ziegler, TSLP: From allergy to cancer. *Nat. Immunol.* **20**, 1603–1609 (2019).
42. P. C. Schwalie, H. Dong, M. Zachara, J. Russeil, D. Alpern, N. Akchiche, C. Caprara, W. Sun, K. U. Schlaudraff, G. Soldati, C. Wolfrum, B. Deplancke, A stromal cell population that inhibits adipogenesis in mammalian fat depots. *Nature* **559**, 103–108 (2018).
43. C. Hepler, B. Shan, Q. Zhang, G. H. Henry, M. Shao, L. Vishvanath, A. L. Ghaben, A. B. Mobley, D. Strand, G. C. Hon, R. K. Gupta, Identification of functionally distinct fibro-inflammatory and adipogenic stromal subpopulations in visceral adipose tissue of adult mice. *eLife* **7**, e39636 (2018).
44. G. Marcelin, A. Ferreira, Y. Liu, M. Atlan, J. Aron-Wisnewsky, V. Pelloux, Y. Botbol, M. Ambrosini, M. Fradet, C. Rouault, C. Hénégar, J. S. Hulot, C. Poitou, A. Torcivia, R. Nail-Barthelemy, J. C. Bichet, E. L. Gautier, K. Clement, A PDGFRα-mediated switch toward $CD9^{high}$ adipocyte progenitors controls obesity-induced adipose tissue fibrosis. *Cell Metab.* **25**, 673–685 (2017).
45. C. Perez-Shibayama, C. Gil-Cruz, H. W. Cheng, L. Onder, A. Printz, U. Mörbe, M. Novkovic, C. Li, C. Lopez-Macias, M. B. Buechler, S. J. Turley, M. Mack, C. Soneson, M. D. Robinson, E. Scandella, J. Gommerman, B. Ludewig, Fibroblastic reticular cells initiate immune responses in visceral adipose tissues and secure peritoneal immunity. *Sci. Immunol.* **3**, eaar4539 (2018).
46. C. Trapnell, D. Cacchiarelli, J. Grimsby, P. Pokharel, S. Li, M. Morse, N. J. Lennon, K. J. Livak, T. S. Mikkelsen, J. L. Rinn, The dynamics and regulators of cell fate decisions are revealed by pseudotemporal ordering of single cells. *Nat. Biotechnol.* **32**, 381–386 (2014).
47. O. Cenaj, D. H. R. Allison, R. Imam, B. Zeck, L. M. Drohan, L. Chiriboga, J. Llewellyn, C. Z. Liu, Y. N. Park, R. G. Wells, N. D. Theise, Evidence for continuity of interstitial spaces across tissue and organ boundaries in humans. *Commun. Biol.* **4**, 436 (2021).
48. D. M. Zaiss, L. Yang, P. R. Shah, J. J. Kobie, J. F. Urban, T. R. Mosmann, Amphiregulin, a TH2 cytokine enhancing resistance to nematodes. *Science* **314**, 1746 (2006).
49. C. M. Minutti, S. Drube, N. Blair, C. Schwartz, J. C. McCrae, A. N. McKenzie, T. Kamradt, M. Mokry, P. J. Coffer, M. Sibilia, A. J. Sijts, P. G. Fallon, R. M. Maizels, D. M. Zaiss, Epidermal growth factor receptor expression licenses type-2 helper T cells to function in a T cell receptor-independent fashion. *Immunity* **47**, 710–722.e6 (2017).
50. B. Yang, T. Kumoto, T. Arima, M. Nakamura, Y. Sanada, T. Kumrungsee, Y. Sotomaru, M. Shimada, N. Yanaka, Transgenic mice specifically expressing amphiregulin in white adipose tissue showed less adipose tissue mass. *Genes Cells* **23**, 136–145 (2018).
51. D. Jiang, Y. Rinkevich, Furnishing wound repair by the subcutaneous fascia. *Int. J. Mol. Sci.* **22**, 9006 (2021).
52. P. C. Benias, R. G. Wells, B. Sackey-Aboagye, H. Klavan, J. Reidy, D. Buonocore, M. Miranda, S. Kornacki, M. Wayne, D. L. Carr-Locke, N. D. Theise, Structure and distribution of an unrecognized interstitium in human tissues. *Sci. Rep.* **8**, 4947 (2018).
53. Y. Lin, G. Leung, D. Louie, A. Bogoslowski, J. Ross, P. Kubes, P. Y. von der Weid, S. Liao, Perinodal adipose tissue participates in immune protection through a lymphatic vessel-independent route. *J. Immunol.* **201**, 296–305 (2018).
54. D. Correa-Gallegos, D. Jiang, S. Christ, P. Ramesh, H. Ye, J. Wannemacher, S. Kalgudde Gopal, Q. Yu, M. Aichler, A. Walch, U. Mirastschijski, T. Volz, Y. Rinkevich, Patch repair of deep wounds by mobilized fascia. *Nature* **576**, 287–292 (2019).
55. J. Sbierski-Kind, N. Mroz, A. B. Molofsky, Perivascular stromal cells: Directors of tissue immune niches. *Immunol. Rev.* **302**, 10–31 (2021).
56. B. A. Shook, R. R. Wasko, G. C. López-Giráldez, E. Salazar-Gatzimas, F. Lopez-Giraldez, B. C. Dash, A. R. Muñoz-Rojas, K. D. Aultman, R. K. Zwick, V. Lei, J. L. Arbiser, K. Miller-Jensen, D. A. Clark, H. C. Hsia, V. Horsley, Myofibroblast proliferation and heterogeneity are supported by macrophages during skin repair. *Science* **362**, eaar2971 (2018).
57. Z. Zhang, M. Shao, C. Hepler, Z. Zi, S. Zhao, Y. A. An, Y. Zhu, A. L. Ghaben, M. Y. Wang, N. Li, T. Onodera, N. Joffin, C. Crewe, Q. Zhu, L. Vishvanath, A. Kumar, C. Xing, Q. A. Wang, L. Gautron, Y. Deng, R. Gordillo, I. Kruglikov, C. M. Kusminski, R. K. Gupta, P. E. Scherer, Dermal adipose tissue has high plasticity and undergoes reversible dedifferentiation in mice. *J. Clin. Invest.* **129**, 5327–5342 (2019).
58. W. J. Sullivan, P. J. Mullen, E. W. Schmid, A. Flores, M. Momcilovic, M. S. Sharpley, D. Jelinek, A. E. Whiteley, M. B. Maxwell, B. R. Wilde, U. Banerjee, H. A. Coller, D. B. Shackelford, D. Braas, D. E. Ayer, T. Q. de Aguiar Vallim, W. E. Lowry, H. R. Christofk, Extracellular matrix remodeling regulates glucose metabolism through TXNIP destabilization. *Cell* **175**, 117–132.e21 (2018).
59. T. Crowley, C. D. Buckley, A. R. Clark, Stroma: The forgotten cells of innate immune memory. *Clin. Exp. Immunol.* **193**, 24–36 (2018).
60. S. C. Cheng, J. Quintin, R. A. Cramer, K. M. Shepardson, S. Saeed, V. Kumar, E. J. Giamarellos-Bourboulis, J. H. Martens, N. A. Rao, A. Aghajanirefah, G. R. Manjeri, Y. Li, D. C. Ifrim, R. J. Arts, B. M. van der Veer, P. M. Deen, C. Logie, L. A. O'Neill, P. Willems, F. L. van de Veerdonk, J. W. van der Meer, A. Ng, L. A. Joosten, C. Wijmenga, H. G. Stunnenberg, R. J. Xavier, M. G. Netea, mTOR- and HIF-1α-mediated aerobic glycolysis as metabolic basis for trained immunity. *Science* **345**, 1250684 (2014).
61. S. Saeed, J. Quintin, H. H. Kerstens, N. A. Rao, A. Aghajanirefah, F. Matarese, S. C. Cheng, J. Ratter, K. Berentsen, M. A. van der Ent, N. Sharifi, E. M. Janssen-Megens, M. Ter Huurne, A. Mandoli, T. van Schaik, A. Ng, F. Burden, K. Downes, M. Frontini, V. Kumar, E. J. Giamarellos-Bourboulis, W. H. Ouwehand, J. W. van der Meer, L. A. Joosten, C. Wijmenga, J. H. Martens, R. J. Xavier, C. Logie, M. G. Netea, H. G. Stunnenberg, Epigenetic programming of monocyte-to-macrophage differentiation and trained innate immunity. *Science* **345**, 1251086 (2014).
62. C. W. Y. Ha, A. Martin, G. D. Sepich-Poore, B. Shi, Y. Wang, K. Gouin, G. Humphrey, K. Sanders, Y. Ratnayake, K. S. L. Chan, G. Hendrick, J. R. Caldera, C. Arias, J. E. Moskowitz, S. J. Ho Sui, S. Yang, D. Underhill, M. J. Brady, S. Knott, K. Kaihara, M. J. Steinbaugh, H. Li, D. P. B. McGovern, R. Knight, P. Fleshner, S. Devkota, Translocation of viable gut microbiota to mesenteric adipose drives formation of creeping fat in humans. *Cell* **183**, 666–683.e17 (2020).
63. C. M. Lo, H. B. Wang, M. Dembo, Y. L. Wang, Cell movement is guided by the rigidity of the substrate. *Biophys. J.* **79**, 144–152 (2000).
64. F. Puttur, L. Denney, L. G. Gregory, J. Vuononvirta, R. Oliver, L. J. Entwistle, S. A. Walker, M. B. Headley, E. J. McGhee, J. E. Pease, M. F. Krummel, L. M. Carlin, C. M. Lloyd, Pulmonary environmental cues drive group 2 innate lymphoid cell dynamics in mice and humans. *Sci. Immunol.* **4**, eaav7638 (2019).
65. H. Lv, L. Li, M. Sun, Y. Zhang, L. Chen, Y. Rong, Y. Li, Mechanism of regulation of stem cell differentiation by matrix stiffness. *Stem Cell. Res. Ther.* **6**, 103 (2015).
66. B. D. Hondowicz, D. An, J. M. Schenkel, K. S. Kim, H. R. Steach, A. T. Krishnamurty, G. J. Keitany, E. N. Garza, K. A. Fraser, J. J. Moon, W. A. Altemeier, D. Masopust, M. Pepper, Interleukin-2-dependent allergen-specific tissue-resident memory cells drive asthma. *Immunity* **44**, 155–166 (2016).
67. C. S. N. Klose, T. Mahlakoiv, J. B. Moeller, L. C. Rankin, A. L. Flamar, H. Kabata, L. A. Monticelli, S. Moriyama, G. G. Putzel, N. Rakhilin, X. Shen, E. Kostenis, G. M. Konig, T. Senda, D. Carpenter, D. L. Farber, D. Artis, The neuropeptide neuromedin U stimulates innate lymphoid cells and type 2 inflammation. *Nature* **549**, 282–286 (2017).
68. V. Cardoso, J. Chesne, H. Ribeiro, B. Garcia-Cassani, T. Carvalho, T. Bouchery, K. Shah, N. L. Barbosa-Morais, N. Harris, H. Veiga-Fernandes, Neuronal regulation of type 2 innate lymphoid cells via neuromedin U. *Nature* **549**, 277–281 (2017).
69. A. Wallrapp, S. J. Riesenfeld, P. R. Burkett, R.-E. E. Abdulnour, J. Nyman, D. Dionne, M. Hofree, M. S. Cuoco, C. Rodman, D. Farouq, B. J. Haas, T. L. Tickle, J. J. Trombetta, P. Baral, C. S. N. Klose, T. Mahlakõiv, D. Artis, O. Rozenblatt-Rosen, I. M. Chiu, B. D. Levy, M. S. Kowalczyk, A. Regev, V. K. Kuchroo, The neuropeptide NMU amplifies ILC2-driven allergic lung inflammation. *Nature* **549**, 351–356 (2017).
70. D.-H. Kim, S. J. Van Dyken, ILC2s in high definition: Decoding the logic of tissue-based immunity. *Trends Immunol.* **41**, 7–16 (2020).
71. D. M. Zaiss, W. C. Gause, L. C. Osborne, D. Artis, Emerging functions of amphiregulin in orchestrating immunity, inflammation, and tissue repair. *Immunity* **42**, 216–226 (2015).
72. N. Arpaia, J. A. Green, B. Moltedo, A. Arvey, S. Hemmers, S. Yuan, P. M. Treuting, A. Y. Rudensky, A distinct function of regulatory T cells in tissue protection. *Cell* **162**, 1078–1089 (2015).
73. C. M. Minutti, R. V. Modak, F. Macdonald, F. Li, D. J. Smyth, D. A. Dorward, N. Blair, C. Husovsky, A. Muir, E. Giampazolias, R. Dobie, R. M. Maizels, T. J. Kendall, D. W. Griggs, M. Kopf, N. C. Henderson, D. M. Zaiss, A macrophage-pericyte axis directs tissue restoration via amphiregulin-induced transforming growth factor β activation. *Immunity* **50**, 645–654.e6 (2019).
74. R. Samarakoon, A. D. Dobberfuhl, C. Cooley, J. M. Overstreet, S. Patel, R. Goldschmeding, K. K. Meldrum, P. J. Higgins, Induction of renal fibrotic genes by TGF-β1 requires EGFR activation, p53 and reactive oxygen species. *Cell. Signal.* **25**, 2198–2209 (2013).
75. L. J. Zhang, C. F. Guerrero-Juarez, T. Hata, S. P. Bapat, R. Ramos, M. V. Plikus, R. L. Gallo, Innate immunity. Dermal adipocytes protect against invasive *Staphylococcus aureus* skin infection. *Science* **347**, 67–71 (2015).
76. B. O. Zhou, H. Yu, R. Yue, Z. Zhao, J. J. Rios, O. Naveiras, S. J. Morrison, Bone marrow adipocytes promote the regeneration of stem cells and haematopoiesis by secreting SCF. *Nat. Cell Biol.* **19**, 891–903 (2017).
77. J. E. Heredia, L. Mukundan, F. M. Chen, A. A. Mueller, R. C. Deo, R. M. Locksley, T. A. Rando, A. Chawla, Type 2 innate signals stimulate fibro/adipogenic progenitors to facilitate muscle regeneration. *Cell* **153**, 376–388 (2013).

78. K. Mohrs, A. E. Wakil, N. Killeen, R. M. Locksley, M. Mohrs, A two-step process for cytokine production revealed by IL-4 dual-reporter mice. *Immunity* **23**, 419–429 (2005).
79. Y. Y. Wan, R. A. Flavell, Identifying Foxp3-expressing suppressor T cells with a bicistronic reporter. *Proc. Natl. Acad. Sci. U.S.A.* **102**, 5126–5131 (2005).
80. C. L. Maynard, L. E. Harrington, K. M. Janowski, J. R. Oliver, C. L. Zindl, A. Y. Rudensky, C. T. Weaver, Regulatory T cells expressing interleukin 10 develop from Foxp3$^+$ and Foxp3$^-$ precursor cells in the absence of interleukin 10. *Nat. Immunol.* **8**, 931–941 (2007).
81. D. R. Herbert, C. Holscher, M. Mohrs, B. Arendse, A. Schwegmann, M. Radwanska, M. Leeto, R. Kirsch, P. Hall, H. Mossmann, B. Claussen, I. Forster, F. Brombacher, Alternative macrophage activation is essential for survival during schistosomiasis and downmodulates T helper 1 responses and immunopathology. *Immunity* **20**, 623–635 (2004).
82. A. Natarajan, B. Wagner, M. Sibilia, The EGF receptor is required for efficient liver regeneration. *Proc. Natl. Acad. Sci. U.S.A.* **104**, 17081–17086 (2007).
83. M. Camberis, G. Le Gros, J. Urban Jr., Animal model of *Nippostrongylus brasiliensis* and *Heligmosomoides polygyrus*. *Curr. Protoc. Immunol.* **Chapter 19**, Unit 19.12 (2003).
84. T. Hashimshony, N. Senderovich, G. Avital, A. Klochendler, Y. de Leeuw, L. Anavy, D. Gennert, S. Li, K. J. Livak, O. Rozenblatt-Rosen, Y. Dor, A. Regev, I. Yanai, CEL-Seq2: Sensitive highly-multiplexed single-cell RNA-seq. *Genome Biol.* **17**, 77 (2016).
85. J. S. Herman, Sagar, D. Grun, FateID infers cell fate bias in multipotent progenitors from single-cell RNA-seq data. *Nat. Methods* **15**, 379–386 (2018).
86. J. Wills, J. Edwards-Hicks, A. J. Finch, AssayR: A simple mass spectrometry software tool for targeted metabolic and stable isotope tracer analyses. *Anal. Chem.* **89**, 9616–9619 (2017).
87. V. Bhardwaj, S. Heyne, K. Sikora, L. Rabbani, M. Rauer, F. Kilpert, A. S. Richter, D. P. Ryan, T. Manke, snakePipes: Facilitating flexible, scalable and integrative epigenomic analysis. *Bioinformatics* **35**, 4757–4759 (2019).
88. F. Ramírez, D. P. Ryan, B. Gruning, V. Bhardwaj, F. Kilpert, A. S. Richter, S. Heyne, F. Dündar, T. Manke, deepTools2: A next generation web server for deep-sequencing data analysis. *Nucleic Acids Res.* **44**, W160–W165 (2016).
89. A. Dobin, C. A. Davis, F. Schlesinger, J. Drenkow, C. Zaleski, S. Jha, P. Batut, M. Chaisson, T. R. Gingeras, STAR: Ultrafast universal RNA-seq aligner. *Bioinformatics* **29**, 15–21 (2013).
90. Y. Liao, G. K. Smyth, W. Shi, featureCounts: An efficient general purpose program for assigning sequence reads to genomic features. *Bioinformatics* **30**, 923–930 (2014).
91. M. I. Love, W. Huber, S. Anders, Moderated estimation of fold change and dispersion for RNA-seq data with DESeq2. *Genome Biol.* **15**, 550 (2014).
92. A. K. Jha, S. C. Huang, A. Sergushichev, V. Lampropoulou, Y. Ivanova, E. Loginicheva, K. Chmielewski, K. M. Stewart, J. Ashall, B. Everts, E. J. Pearce, E. M. Driggers, M. N. Artyomov, Network integration of parallel metabolic and transcriptional data reveals metabolic modules that regulate macrophage polarization. *Immunity* **42**, 419–430 (2015).
93. T. Stuart, A. Butler, P. Hoffman, C. Hafemeister, E. Papalexi, W. M. Mauck III, Y. Hao, M. Stoeckius, P. Smibert, R. Satija, Comprehensive integration of single-cell data. *Cell* **177**, 1888–1902.e21 (2019).
94. H. Li, R. Durbin, Fast and accurate long-read alignment with Burrows-Wheeler transform. *Bioinformatics* **26**, 589–595 (2010).
95. D. Grun, L. Kester, A. van Oudenaarden, Validation of noise models for single-cell transcriptomics. *Nat. Methods* **11**, 637–640 (2014).
96. D. Grün, M. J. Muraro, J. C. Boisset, K. Wiebrands, A. Lyubimova, G. Dharmadhikari, M. van den Born, J. van Es, E. Jansen, H. Clevers, E. J. P. de Koning, A. van Oudenaarden, De novo prediction of stem cell identity using single-cell transcriptome data. *Cell Stem Cell* **19**, 266–277 (2016).
97. L. Ferrer-Font, P. Mehta, P. Harmos, A. J. Schmidt, S. Chappell, K. M. Price, I. F. Hermans, F. Ronchese, G. le Gros, J. U. Mayer, High-dimensional analysis of intestinal immune cells during helminth infection. *eLife* **9**, e51678 (2020).

**Acknowledgments:** We would like to thank M. Wilson, A. Akhtar, M. Seidl, R. Maizels, P. Murray, S. Eming, A. Roers, A. Kiemen, A. Kania and D. Vöhringer for reagents, advice, and discussions and A. Quintana, J. Sutherland, and F. Haessler for help with mouse breeding. We acknowledge the Johns Hopkins University School of Medicine Microscope Facility, the Johns Hopkins University Oncology Tissue Services, the Institute of Clinical Pathology, University of Freiburg, and the Flow Cytometry, DeepSequencing, and Bioinformatics facilities at the MPI-IE for technical support and constructive criticism. **Funding:** This study was supported by NIH grant AI 110481 (to E.J.P.), German Research Foundation grant DFG FOR 2599 (to E.J.P. and A.M.K.), German Research Foundation grant under Germany's Excellence Strategy CIBSS EXC-2189 Project ID 390939984 (to D.G.), German Research Foundation grant SPP1937 GR4980/1-1 (to D.G.), Alexander von Humboldt Fellowship Foundation (to A.M.K., M.V., F.B., and J.C.), CAPES/Alexander von Humboldt Fellowship Foundation grant 88881.136065/2017-01 (to A.C.), Marie Skłodowska-Curie Action Individual Fellowship MSCA-IF (to F.B. and J.C.), European Research Council Advanced grant ERC-2015-AdG TNT-Tumors 694883 (to M.S.), European Union's Horizon 2020 research and innovation program under Marie Skłodowska-Curie grant agreement no. 766214 Meta-Can (to M.S.), two Bloomberg Distinguished Professorships from Johns Hopkins University (E.J.P. and E.L.P.), and the Max Planck Society. **Author contributions:** Conceptualization: A.M.K., D.E.S., J.A.P., E.L.P., and E.J.P. Methodology: D.E.S., P.Z., N.R., J.E.-H., and D.G. Investigation: A.M.K., A.H., K.M.G., P.Z., L.D., R.K., G.C., J.D.C., A.C., M.V., F.B., and J.C. Visualization: A.M.K., F.B., D.E.S., and P.Z. Funding acquisition: E.L.P. and E.J.P. Resources: J.F.U. and M.S. Writing—original draft: A.M.K. and E.J.P. Writing—review and editing: A.M.K., A.H., D.E.S., P.Z., K.M.G., R.K., G.C., M.V., J.C., M.S., J.A.P., J.F.U., D.G., E.L.P., and E.J.P. Supervision: E.J.P. **Competing interests:** E.J.P. and E.L.P. are founders of Rheos Medicines. E.L.P. is a SAB member of ImmunoMet Therapeutics. D.G. is a SAB member of Gordian Biotechnology. G.C. is a senior editor at *Nature* and an employee of *Springer Nature*. The other authors declare that they have no competing interests. **Data and materials availability:** The RNA-seq data generated in this study have been deposited in the Gene Expression Omnibus (GEO) repository (accession number: GSE157314). All other data needed to evaluate the conclusions in the paper are present in the paper or the Supplementary Materials.

Submitted 12 June 2022
Accepted 31 August 2022
Published 14 October 2022
10.1126/sciimmunol.add3263

Science Immunology

# Resident $T_H2$ cells orchestrate adipose tissue remodeling at a site adjacent to infection

Agnieszka M. Kabat, Alexandra Hackl, David E. Sanin, Patrice Zeis, Katarzyna M. Grzes, Francesc Baixauli, Ryan Kyle, George Caputa, Joy Edwards-Hicks, Matteo Villa, Nisha Rana, Jonathan D. Curtis, Angela Castoldi, Jovana Cupovic, Leentje Dreesen, Maria Sibilia, J. Andrew Pospisilik, Joseph F. Urban, Jr., Dominic Grn, Erika L. Pearce, and Edward J. Pearce

*Sci. Immunol.*, **7** (76), eadd3263.
DOI: 10.1126/sciimmunol.add3263

**Adipose tissue affects parasitic infection**
Adipose tissue has been linked to immune responses and protection against infection, but how it contributes to parasitic helminths remains unclear. Here, Kabat *et al.* used RNA-seq, metabolomics, flow cytometry, and histology to study the adipose tissue from mice infected with intestinal *Heligmosomoides polygyrus*. They found that helminth gut infection reduced mesenteric adipose tissue, which associated with increased infiltration of resident $T_H2$ CD4+ T cells that produced TGF# and amphiregulin. Via these factors, resident $T_H2$s communicated with thymic stromal lymphopoietin and IL-33–producing stromal cells in the collagen-rich interstitial spaces of the mesenteric adipose tissue. Disrupting amphiregulin signaling in stromal cells led to worse *H. polygyrus* infection. Thus, $T_H2$ and stromal cells communicate in the adipose tissue, contributing to anti-parasite immunity.